J Civil Struct Health Monit (2015) 5:655–676
DOI 10.1007/s13349-015-0146-3

ORIGINAL PAPER

Long-term structural monitoring of the damaged Basilica S. Maria di Collemaggio through a low-cost wireless sensor network

Francesco Potenza[1] · Fabio Federici[2] · Marco Lepidi[3] · Vincenzo Gattulli[1] · Fabio Graziosi[2] · Andrea Colarieti[2]

Received: 10 July 2015 / Revised: 8 September 2015 / Accepted: 19 October 2015 / Published online: 4 November 2015

Abstract The work presents the inter-disciplinary multi-year project focused on the permanent seismic monitoring of a historical structure, the Basilica S. Maria di Collemaggio, by means of an advanced wireless sensor network. Considered among the architectural masterpieces of the Italian Romanesque, the structural behaviour of the monumental masonry church is strongly debated after the heavy damages and the partial collapse that occurred during the 2009 L'Aquila earthquake. From the perspective of information technology, critical issues in the wireless data acquisition and communication are analysed. The sensor network design, deployment and performance are discussed with respect to the high-demanding service requirements—as well as the non-negligible management costs—specifically related to the long-term monitoring of a monumental masonry structure in a seismic area. From the perspective of experimental signal analysis, the acceleration data collected during a 3-year period of seismic monitoring are analysed in the frequency and time domains. The results allow the clear detection of complex interactions between the masonry structures and some of the temporary protective installations. Stochastic subspace identification procedures are applied, with critical analysis of their effectiveness in the assessment of reliable modal models from the building response to real seismic events. Finally, the robustness of the modal identification obtained from the structural responses to different near- and far-field micro-earthquakes is discussed, with the aid of numerical models of the damaged and protected church configuration.

Keywords Seismic structural monitoring · Wireless sensor network · Stochastic subspace identification · Cultural heritage · Monumental structures

1 Introduction

Direct static and dynamic response measurements are nowadays becoming easily obtainable by permanently installing inexpensive sensor networks based on wireless communications. Civil infrastructures and historic structures, essential for the social and economic prosperity of a territory, constitute a peculiar and challenging framework for the deployment of smart sensor technologies, which may represent a significant enhancement in support of structural health and safety assessments based on traditional sensors or expert visual inspections.

Recent developments in micro-electro-mechanical systems (MEMS), wireless communications, and digital electronics are producing low-cost, power-saving sensor nodes that are small in size, communicate untethered across short distances and possess multifunctional features [1]. In comparison, wired monitoring systems are typically implemented in buildings and infrastructures with a relatively higher cost per channel. Such a unitary cost can quickly grow up along with the logistical and operational

✉ Francesco Potenza
francesco.potenza@cc.univaq.it

Vincenzo Gattulli
vincenzo.gattulli@univaq.it

[1] Department of Civil Architectural and Environmental Engineering, University of L'Aquila, Via Giovanni Gronchi, 67100 L'Aquila, Italy

[2] DEWS, Center of Excellence, Nucleo Industriale di Pile, University of L'Aquila, 67100 L'Aquila, Italy

[3] Department of Civil, Chemical and Environmental Engineering, University of Genoa, Via Montallegro 1, 16145 Genoa, Italy

difficulties inherent in the network deployment. Smart sensors, which can include onboard communication, processing and memory features, can conjugate the cheapness of the deployment and installation procedures with the richness of the communicated information [2, 3].

In the last decade, wireless communications, low-power computing and sensing technology have overcome several technical problems, permitting the monitoring of different typologies of civil infrastructures using wireless sensor networks (WSNs) [4]. Among these, historic constructions represent rare exceptions, with only a single case concerning a medieval tower reported in the literature [5]. However, the use of this technology is slowly becoming more widespread and pervasive.

Although the advances have been slowed down due to the complexity of programming smart sensors, the availability of open-source frameworks for structural health monitoring (SHM) using WSNs has partially solved this bottleneck [6], leading to the recent implementation of real-time wireless data acquisition [7].

Despite the extraordinary development of WSNs-based SHM systems, their mature establishment as successful operational tools still implies post-processing procedures of data analysis and structural models suitable to describe the mechanical behavior of the monitored structures, capture the time-dependent degradation of the structural performance and formulate safety evaluations. If available, the eventual development of automated WSN systems capable of assessing the behavior of structures during and immediately after earthquakes—even when they are accompanied by a low energy release—, will be particularly valuable for mitigating the high risks for the human safety, the cultural heritage and the economic stability associated with seismic areas.

The effective formulation, identification or updating of reliable dynamic models, however, is a rather involved process. The complexity of the structural behavior under earthquake loadings has been evidenced since the earlier studies of the direct nonlinear problem [8], whereas the solution of the inverse problem, even for the identification of a linear model, should take into account that the dynamic response is a nonlinear function of the parameters. A basic route for determining an appropriate structural model is to use an output-error approach in which a measure-of-fit is defined and the unknown parameters are estimated through optimization algorithms; this permits the creation of a system realization capable of reproducing the initial input–output relations [9]. Following a time-domain formulation, the Eigensystem Realization Algorithm (ERA) for modal parameter identification and model reduction of linear dynamic systems has been proposed [10]. According to this approach, a minimal realization that simulates the system response to a unit pulse inputs is identified.

Concurrent with the development of ERA, research interest towards system identification has also rapidly increased in the seismic engineering field, where the main concerns regarded the non-stationary nature of earthquake excitation, which does not comply with the basic hypotheses of many vibration-based identification procedures. Moreover, the adequacy of a linear prediction model as suited framework for structural analysis has been discussed through a comparative study of different identification techniques, which study has pointed out that simple and reliable algorithms are necessary elements of a broader strategy for control or damage assessment [11].

In addition, the goal of finding dynamic models for input–output data generated by a linear, time-invariant, finite-dimensional, dynamic system with both deterministic and stochastic input signals has been newly approached by means of geometric tools. They are based on the concept of subspace identification, which reflects the fact that linear models can be obtained from row and column spaces of certain matrices, calculated from input–output data [12]. A number of improvements in this area of linear parametric identification has been proposed to take into account either the characteristics of the excitation (as in the case of earthquake [13]), or the effects of considering reference outputs [14], or to evidence and compare the differences in the most common parametric identification procedures working in the time domain. These include, for example: instrumental variable (IV), ERA, and stochastic subspace identification (SSI), both covariance-driven (SSI-COV) and data-driven (SSI-DATA) [15, 16]. With an understanding of the drawbacks and features of all these techniques, an effort towards the possible simultaneous use of artificial and ambient excitations has also been recently carried out, thoroughly exploiting the potential of SSI-based procedures [17].

The present paper deals with the key issues that emerged from an ongoing inter-disciplinary research project focused on the development of a fully functional, easily manageable and economically affordable systems for the permanent structural health monitoring (SHM) of civil and historical structures, specifically in seismic areas. The research is based on the valuable experience acquired during the design, deployment, test and management of a wireless sensor network for the structural monitoring of a medieval masonry structure, the Basilica S. Maria di Collemaggio. Considered one of the architectural masterpieces of the Italian Romanesque, the church was founded in 1287. Its importance in religious history is related to the only papal coronation outside Rome (Pope Celestine V, 1294), and the presence of the first Holy Door, seat of a yearly jubilee. The research findings are also intended as a contribution to the rather heated debate about the structural behaviour of the monumental masonry church, after the

heavy damages and the partial collapse that occurred during the 2009 L'Aquila earthquake [18–20]. Furthermore, the test-bench represented by the seismic monitoring a monumental masonry structure deeply damaged by an earthquake offers a unique add-on to an open field of structural dynamics and earthquake engineering. Indeed, due to the high seismic activity of the site [21, 22], the monitoring system was specifically designed for seismic and dynamic response analyses based on acceleration, crack opening and wall inclination measurements. Three years of monitoring data are presented, with discussion of their suitability for the parametric identification of a reliable numerical models of the church behavior under moderate and micro-earthquakes.

The paper is structured as follows: Section 2 describes the rapid evolution of the technology of wireless sensor networks for structural monitoring of infrastructure, focusing on the main features relevant to the proposed implementation. Section 3 briefly describes the operational scenario and furnishes details on the implementation of the monitoring networks. Section 4 poses the direct and inverse problem, with regard to which a parametric identification methodology defined directly in the time domain, namely the SSI approach, is discussed in view of a massive accumulation of noisy data coming from the 3-year monitoring of the monumental structure. Section 5 discusses the results obtained from preliminary tests both in the lab and on the site, as well as the spectral content of the typical acceleration measurements acquired by the system during seismic events. Section 6 discusses the results of employing the SSI process to identify modal models from 3 years of measurements of earthquake-induced vibrations of the monument. In Sect. 7 is performed the manual modal updating. Finally, some concluding remarks are pointed out.

2 Wireless sensor networks for SHM

Traditional structural monitoring systems consist of grids of sensors deployed throughout the target structure and connected to a central processing unit by means of a wired communication infrastructure. Usually, each sensor communicates with a central data acquisition system through a coaxial cable. Wired systems are currently widely used in civil engineering, even though they present several practical disadvantages. These systems are not flexible and, in the case of large structures, the deployment of the wires may be difficult. The wires and their related installation costs often turn out to be the major component of the total cost of a monitoring system [1–3, 23]. Moreover, traditional monitoring systems are usually based on bulk sensors (e.g. bulk force-balance accelerometers). Typically, these sensors have a large footprint and are expensive. Nevertheless, this type of system is still widely used in civil engineering for operational modal analyses and temporary monitoring setups. Applications of this technology on famous monumental buildings includes, for example, a setup composed of 20 piezo-electric accelerometers and a 30-channel data acquisition system used in a 2-year monitoring of the Anime Sante Church in L'Aquila, Italy [24], and a similar setup implemented by the same individual, but comprising only three accelerometers, used to monitor the historic masonry facade of Palazzo Ducale in Venice, Italy [25]. In another case, a set of 25 accelerometers, arranged in ten different measurement points, has recently been used to measure traffic-induced vibration in the Basilica of Maxentium in Rome, Italy [26].

In recent years, there has been a progressive development in the integration of electronic devices, wireless communications and the miniaturization of sensors. Continuous improvements in integration and low voltage, low-power design of microprocessors and embedded microcontrollers allow higher computational performances with a gradual reduction of energy consumption [3]. In telecommunications, there has been a gradual decline in device cost and a progressive improvement in personal area network communication standards. Finally, the development of innovative fabrication technologies, such as MEMS (micro-electro-mechanical systems), have allowed for the increasing miniaturization of sensors with a significant reduction of power consumption.

A wireless sensor network is a network of heterogeneous devices (sensor nodes, or motes) in which each node is able to record physical data from its environment, process the acquired data, and communicate with its neighbors. Sensor nodes are usually battery powered and thus can operate without any wired external connection. In order to run on battery power for prolonged periods, sensor nodes must have extremely low power consumption.

Wireless sensor networks are used in various operational scenarios, from real-time tracking of moving objects to the monitoring of environmental phenomena and spatially distributed processing.

In recent years, the advantages of using wireless sensor networks in structural health monitoring have been increasingly explored [27]. Wireless sensor networks are particularly suited for the implementation of output-only identification techniques, since in this case the measurement of the structural response to environmental excitation is all that is required. In the case of large structures, the use of wireless sensor networks for output-only analysis can be very convenient, since it is possible to deploy a large number of (low cost) sensor nodes along the structure. The first study presented in literature is the structural monitoring of the Alamosa Canyon Bridge (1998) [28]. Other

notable examples are the monitoring of Geumdang and Jindo Bridges in Korea [29, 30], and the Golden Gate Bridge in the USA [31]. In the literature, only a limited number of wireless monitoring system applications are presented for the case of large masonry buildings. Examples include the monitoring project for the Torre Aquila (Aquila Tower) in Trento, Italy [5] and the modal analysis of the chimneys at the Paço dos Duques de Braganza (Palace of the Dukes of Braganza) in Guimaraes, Portugal [32].

3 Seismic monitoring of the Basilica of Santa Maria di Collemaggio

The Basilica of Santa Maria di Collemaggio is the most important church in the city of L'Aquila. The church has a central nave, which measures 61 m in length and 11.3 m in width, and two side aisles measuring 7.8 and 8.0 m in width, respectively. Naves and side aisles are separated by two series of seven columns with a height of 5.3 m and an average central section of about 1 m in diameter. Four external walls, with a masonry thickness varying from 0.95 to 1.05 m are connected on two sides with the church façade and transept area. Other adjacent structures are partially connected with the main body of the Basilica: an octagonal tower is connected on one side of the façade, and another masonry building runs adjacent along about 40 % of the external walls. The church has a wooden roof supported by trusses placed in a cross-sectional direction with respect to the external walls. The dynamic behavior of the Basilica was characterized in numerical and experimental studies conducted before the occurrence of the 2009 L'Aquila earthquake. The earthquake caused a partial collapse of the structure in the transept area [18–20].

After the earthquake, a permanent structural monitoring system was developed and installed inside and outside the damaged church. The main goals of this project were (1) to investigate the possible causes of the collapse; (2) to monitor the performance of the scaffolding structures and other provisional reinforcements (tendons between the walls and temporary composite tape wrapped around the columns for confinement, see Fig. 1); (3) to early detect and prevent the progression of damage, and (4) to make a long-term analysis of the structure dynamic response (including seasonal environmental effects) and its modification after final retrofitting and reconstruction. In order to explore possible advantages of innovative technologies (e.g. wireless communication and smart sensing elements), the monitoring system was based on a wireless sensor network. The main investigation technique selected was analysis of the building dynamic response to ambient actions and low-amplitude seismic events. Sixteen sensor nodes were installed in the church on June 2011. The majority of sensor nodes was placed inside the structure: ten along the main nave, one at the base of a column, and one in the transept area. Two sensor nodes were placed outside, at the top corners of the church's rear facade. Figure 2 illustrates the sensor locations.

The main monitoring platform is based on a wireless communication platform (MEMSIC Imote2 mote) along with a structural monitoring oriented daughter board (MEMSIC SHM-A sensor board). The Imote2 wireless communication platform includes an advanced processing module (Intel Xscale PXA271) and an IEEE 802.15.4 compliant radio transceiver (Texas Instruments CC2420). The MEMSIC SHM-A board features an advanced 16-bit data acquisition system (QuikFilter QF4A512 model) and a MEMS tri-axial accelerometer (ST microelectronics LIS344ALH). Table 1 presents relevant performance characteristics of the MEMS accelerometer. The board also includes a temperature and humidity sensor (Sensirion SHT11) and a luminosity sensor (TAOS 2561), allowing characterization of environmental parameters.

The developed nodes' firmware is based on ISHMP Toolsuite, an open source, service-oriented software library enabling vibration data processing and dynamic response characterization and analysis. ISHMP Toolsuite has been developed in the context of the Illinois Structural Health Monitoring Project (ISHMP), a project specifically oriented to the development of reliable wireless smart sensors for structural monitoring of civil infrastructures [6]. The ISHMP Toolsuite is based on the TinyOS 1.x operating system and specifically targets the Imote2 node and the SHM-A board. The Collemaggio setup actively relies on the Foundation Services, FTSP-based synchronization service and AODV multi-hop routing service from ISHMP Toolsuite. The first service is coupled with a post-processing algorithm for the correction of data synchronization errors [33]. The use of these software components allowed the synchronization error to less than 10 μs, which can be considered the limit values sufficient to preserve the accuracy of the structural analysis and to avoid phase errors in identified mode shapes.

The network gateway is based on the ACME FOX Board G20, a single-board computer built around the Atmel AT91SAM9G20 microcontroller. The board runs on a Debian GNU/Linux distribution and supports the connection of USB peripheral devices and network communication devices (by means of an Ethernet port).

The FOX board communicates with two devices: a 3G modem/router and an Imote2 node. The 3G modem/router provides internet access for automatic uploading of the measurement results to a remote server. In addition, it supports local Wi-Fi connectivity for direct access to the monitoring system. This feature is useful when performing

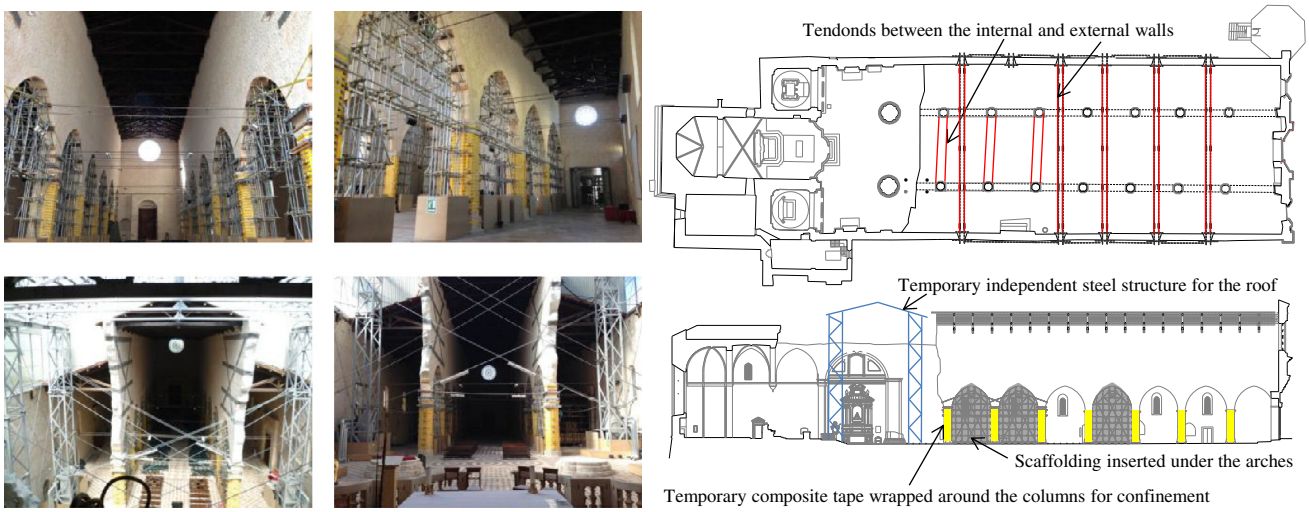

Fig. 1 Scaffolding system and other reinforcements. *Highlighted* in the lateral sections are independent steel structures required to implement a temporary roof

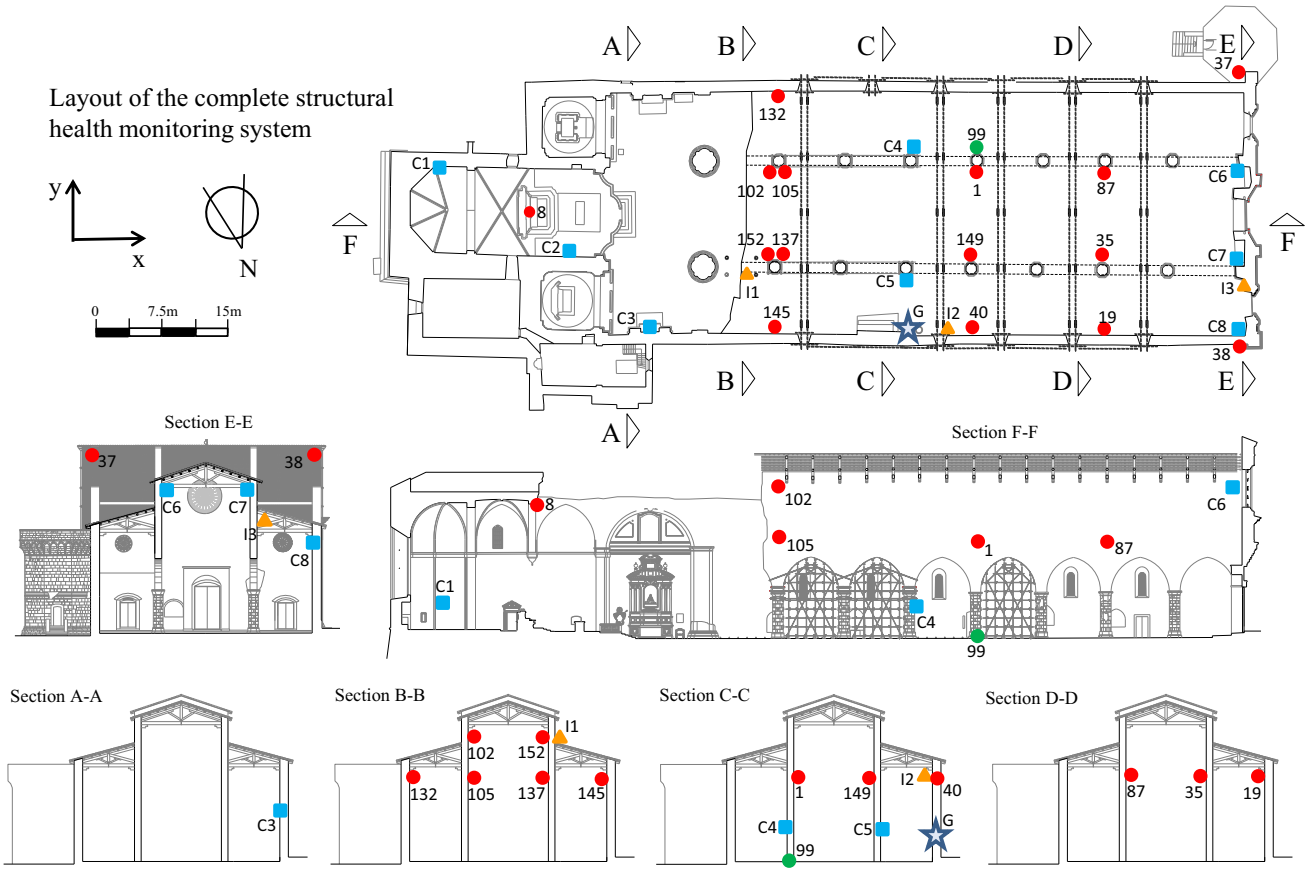

Fig. 2 Location of the multifunction wireless sensors: 16 accelerometers (15 in elevation, *red circle*, and 1 on the ground, *green circle*), 8 extensometers (*blue squares*), 3 wall inclinations (*orange triangles*), and 1 node gateway (*star*) (color figure online)

local tests (since the operator does not need internet access to interact with the network) and as a backup redundant system in case of 3G network access failure. The Imote2 node acts as a network sink, collecting measurement data from other network nodes. Moreover, it forwards operating commands from the gateway to the leaf nodes.

Table 1 LIS344ALH mechanical characteristics

Feature	Value
Input range	±2, ±6 g
Sensitivity	$V_{dd}/5$ @ ±2 g
	$V_{dd}/15$ @ ±6 g
Bandwidth	1.8 kHz
Noise density	50 μg/$\sqrt{}$Hz
Non-linearity	±0.5 % FS
Cross axis	±2 %

The central gateway runs a measurement-scheduling application, which automatically handles data acquisition on leaf nodes, measured-data collection, data compression and load on a remote server machine. Data can be downloaded as compressed archives, or visualized in graphic or text format.

Both the gateway subsystem and leaf nodes are powered by the existing electrical lines. This choice, apparently counterintuitive, has two main motivations. First, the goal of measuring the dynamic response in a time interval as wide as possible preventing the system from any interruption due to the use of duty-cycling energy savings techniques. Second, the goal of avoiding any maintenance intervention (such as node battery replacement) which would require the use of heavy-duty vehicles (trucks and cranes are needed to reach the heights at which sensor nodes are placed), and such vehicles had to be avoided given the precarious state of the Basilica. The continuity of monitoring system operability is guaranteed by an Uninterruptible Power Supply Device. A scheduling algorithm able to alternate two groups of nodes in the mentioned operation (every 15 min) was developed within the project. In this way, continuous coverage of the dynamic response of the building was obtained. The nodes belonging to the groups I are: 105, 102, 1, 87, 132, 37, 8, and 99 (the last is the sensor node placed on the ground), while these belonging to the group II are: 137, 152, 149, 35, 145, 40, 19, and 38.

A second monitoring network including extensometer and inclinometer sensors was also installed in the Basilica (see Fig. 2). Some of the limitations described above, along with the end of the commercial life cycle of the Imote2 platform, led to the development of a novel, custom sensing platform. This developed wireless sensing platform (WESTmote [34]) was installed in the Basilica in July 2013. The node is based on Atmel Zigbit 900 module, which features Atmel AT86RF212, an IEEE 802.15.4 compliant radio transceiver working in the 868 MHz frequency band. The software stack fully implements the IEEE 802.15.4 protocol stack. Nodes are battery powered: this choice is appropriate in the case of the crack width and inclination measurements, as the reduced measurement frequency allows for an extensive use of duty cycle power saving techniques (Fig. 3).

4 Seismic induced vibrations: direct and inverse problems

4.1 Direct problem

The preliminary solution of the direct dynamic problem generally furnishes the insights requisite to designing a suitable experimental setup for the identification and model updating of a given structure. The dynamic behavior of a structure can be described through more or less approximate discretized models of elastic continua (e.g. finite element models).

According to this approach, the system dynamics is generally governed by a set of ordinary differential equations (ODEs) in time, in a certain number n of nodal variables. Therefore, under the hypothesis of linearized kinematics and linear elasto-viscous material behavior, the equation of motion of a structural system can be described by a system of n-ODEs:

$$\mathbf{M}(\ddot{\mathbf{u}}_g(t) + \ddot{\mathbf{u}}(t)) + \mathbf{C}\dot{\mathbf{u}}(t) + \mathbf{K}\mathbf{u}(t) = \mathbf{f}(t) \tag{1}$$

in which $\mathbf{u}$, $\dot{\mathbf{u}}$ and $\ddot{\mathbf{u}}$ are the configuration vector of nodal relative displacements, velocities and accelerations whereas $\mathbf{M}$, $\bar{\mathbf{C}}$ and $\mathbf{K}$ are the mass, damping and stiffness matrices, respectively. Finally $\mathbf{f}(t)$ is the vector of the external nodal forces and $\ddot{\mathbf{u}}_g(t)$ is a complete vector of imposed accelerations due to the ground motion.

The effect of a rigid motion affecting only the translational degree-of-freedom can be considered through the use of a location matrix, $\mathbf{L}$, which permits the reduction of the imposed accelerations to the translational components $\mathbf{a}_g(t)$ through $\ddot{\mathbf{u}}_g(t) = \mathbf{L}\mathbf{a}_g(t)$. Moreover, if only one component of the imposed translational acceleration is considered, a simplified expression is $\mathbf{L}\mathbf{a}_g(t) = \mathbf{L}\mathbf{r}a_g(t)$, where the boolean column vector $\mathbf{r}$ is selecting a specific direction. Similarly, the effect of a generic dynamic load may also be considered as $\mathbf{f}(t) = \mathbf{f}\,f(t)$, that is, the product of its spatial distribution $\mathbf{f}$ and time history $f(t)$. The analytical solution of Eq. (1) can be pursued performing modal analysis of the associated autonomous system and assuming proportional viscous damping. Then the system equations can be decoupled in n independent ODEs governing the modal amplitudes z_i in time, as

$$\ddot{z}_i(t) + 2\omega_i\xi_i\dot{z}_i(t) + \omega_i^2 z_i(t) = \gamma_i^l f(t) - \gamma_i^g a_g(t) \tag{2}$$

where $\omega_i^2 = \frac{K_i}{M_i}$ and $\xi_i = \frac{C_{2i}}{2\sqrt{K_i M_i}}$ are the undamped natural (squared) ith frequency and the ith damping ratio, while M_i, K_i, C_{2i} are the ith mass, stiffness and damping modal parameters, respectively. The terms γ_i^l and γ_i^g are the ith modal participation factors for a generic dynamic load and a unidirectional seismic load, and have the following expression

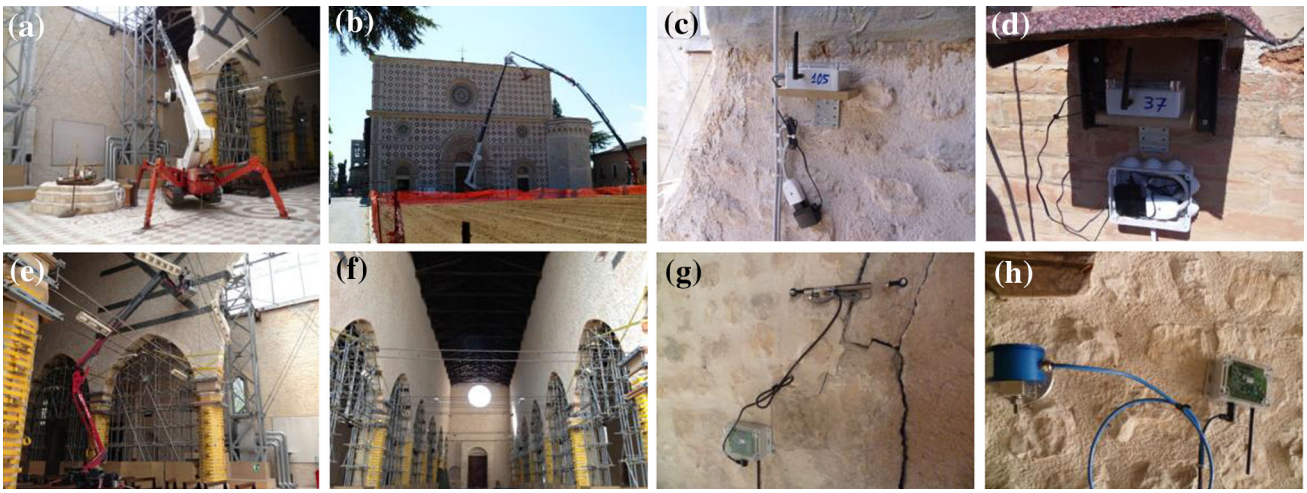

Fig. 3 Installation phases of the accelerometer, extensometer and inclinometer monitoring system. Accelerometer positioning: **a** internal, **b** external. Sensor views: **c** on the internal walls, **d** on a corner of the main façade. **e** Extensometer and inclinometer positioning. **f** Internal view. **g** Extensometer on the internal walls. **h** Inclinometer

$$\gamma_i^l = \frac{\varphi_i^{\mathrm{T}}\mathbf{f}}{\varphi_i^{\mathrm{T}}\mathbf{M}\varphi_i} \qquad \gamma_i^g = \frac{\varphi_i^{\mathrm{T}}\mathbf{MLr}}{\varphi_i^{\mathrm{T}}\mathbf{M}\varphi_i} \tag{3}$$

where φ_i is the ith modal vector. Notice that the Eq. (2) can be normalized with respect to the modal participating factor and considering only the case of the imposed ground motion ($\mathbf{f} = \mathbf{0}$) it can be rewritten

$$\ddot{D}_i(t) + 2\omega_i\xi_i\dot{D}_i(t) + \omega_i^2 D_i(t) = -a_g(t) \tag{4}$$

where consequently the ith modal contribution to the nodal displacements can be written as

$$\mathbf{u}_i(t) = \varphi_i z_i(t) = \gamma_i^g \varphi_i D_i(t) \tag{5}$$

while for the nodal accelerations it can be easily put into relation with the modal response pseudo-acceleration A_i

$$\ddot{\mathbf{u}}_i(t) = \varphi_i \ddot{z}_i(t) = \gamma_i^g \varphi_i \ddot{D}_i(t) = \gamma_i^g \varphi_i A_i(t) \tag{6}$$

and their peak values, indicated by subscript "o", assumes the following expression

$$\ddot{\mathbf{u}}_{io} = \max_t |\ddot{\mathbf{u}}_i(t)| = \gamma_i^g \varphi_i A_{io} \tag{7}$$

The solution of Eq. (2) can be obtained by the classical response spectrum analysis, which is used to determine the normalized peak response spectrum acceleration A_{io} of the simple oscillator for a given natural period (or frequency) and damping ratio. The analysis of the direct dynamic problem evidences that, depending on the structural types (frame-type structure, monumental masonry structure, etc.), significant differences in the seismic modal participation factor γ_i^g may determine substantial different modal contributions to the accelerations. Therefore, the expected level of vibrations in a given point of a structure heavily depends on the modal participation factors and on the associated (in terms of period) normalized peak response spectrum acceleration A_{io}. In typical monumental masonry structures, several modes, the higher of them associated to less excited high-frequencies, are often involved in vibrations due to imposed base motion. Generally, small participation factors are encountered with these numerous modes. Consequently the monuments are prone to small amplitude oscillations and limited base shear ratio with respect to the weight, as has been shown for the Basilica of Collemaggio in comparison with a reinforced concrete building in [35] or for four different churches at L'Aquila in [19], as well as for the Basilica of Maxentius in [26]. Therefore, in the case of structural vibrations due to traffic loads or micro-seismic events, the noise-to-signal ratio is acceptably low only in a few measurement points, to be taken as a reference, while it is significant elsewhere. Moreover, if the system is permanently monitoring the structure, the identification process should properly consider the valuable possibility of direct ground acceleration measurements.

Then, defining a state vector as $\mathbf{x} = [\mathbf{u}^{\mathrm{T}}, \dot{\mathbf{u}}^{\mathrm{T}}]^{\mathrm{T}}$, Eq. (1) can be converted into

$$\dot{\mathbf{x}}(t) = \mathbf{A}_c\mathbf{x}(t) + \mathbf{B}_c\mathbf{a}_g(t) + \mathbf{E}_c\mathbf{f}(t) \tag{8}$$

where the state matrices $\mathbf{A}_c$, $\mathbf{B}_c$ and $\mathbf{E}_c$ are

$$\mathbf{A}_c = \begin{bmatrix} 0 & \mathbf{I} \\ -\mathbf{M}^{-1}\bar{\mathbf{C}} & -\mathbf{M}^{-1}\mathbf{K} \end{bmatrix} \quad \mathbf{B}_c = \begin{bmatrix} 0 \\ -\mathbf{L} \end{bmatrix} \quad \mathbf{E}_c = \begin{bmatrix} 0 \\ \mathbf{M}^{-1} \end{bmatrix} \tag{9}$$

evidencing the difference in the location matrices of the seismic accelerations $\mathbf{B}_c$ with respect to the generic force distribution $\mathbf{E}_c$, which requires the inversion of the mass matrix. It can be posed that the measured quantities, grouped in an output vector $\mathbf{y}(t)$, are generally linear combinations of displacements, velocities or accelerations in a given point (which means a given node in the finite element model)

$$\begin{aligned}\mathbf{y}(t) &= \mathbf{C}_a\ddot{\mathbf{u}}(t) + \mathbf{C}_v\dot{\mathbf{u}}(t) + \mathbf{C}_d\mathbf{u}(t) \\ &= [\mathbf{C}_d - \mathbf{C}_a\mathbf{M}^{-1}\mathbf{K}|\mathbf{C}_v - \mathbf{C}_a\mathbf{M}^{-1}\bar{\mathbf{C}}]\mathbf{x}(t) \\ &\quad - \mathbf{C}_a\mathbf{L}\mathbf{a}_g(t) + \mathbf{C}_a\mathbf{M}^{-1}\mathbf{f}(t)\end{aligned} \tag{10}$$

where C_a, C_n, C_d are the coefficients matrices of the linear combination.

4.2 Inverse problem: system identification of a state-space model

In time-discrete form, the state space differential model represented by Eqs. (8) and (10) is replaced by the following time-discrete model

$$\mathbf{x}_{k+1} = \mathbf{A}\mathbf{x}_k + \mathbf{B}\mathbf{g}_k + \mathbf{E}\mathbf{f}_k + \mathbf{w}_k \tag{11}$$

$$\mathbf{y}_k = \mathbf{C}\mathbf{x}_k + \mathbf{D}\mathbf{g}_k + \mathbf{H}\mathbf{f}_k + \mathbf{v}_\mathbf{k} \tag{12}$$

In which $\mathbf{x}_k$ and $\mathbf{x}_{k+1}$ are the state space vectors at time-step k and $k+1$, respectively, $\mathbf{y}_k$ is the output vector, while $\mathbf{A}$ and $\mathbf{C}$ are the unknown state and the output matrix, respectively. The measured input terms, ground acceleration vector $\mathbf{g}_k$ and loading force vector $\mathbf{f}_k$ are assumed to be noise-free while the system matrices $\mathbf{B}$, $\mathbf{D}$, $\mathbf{E}$, $\mathbf{H}$ are unknown input matrices. Normally, not all forces applied to structures can be measured and often the measurement noise on the output cannot be neglected. Therefore the model is completed by adding two (uncorrelated) stochastic terms, the process vector $\mathbf{w}_k$, and the measurement noise vector $\mathbf{v}_k$. Since the input given by ambient excitation is unknown and can be supposed to lack any dominant harmonic component, it is implicitly included in the noise terms, which are assumed to be zero mean, white vector sequences. In view of the identification of the state-space model in the case of seismic data, it can be reasonably assumed that the seismic action prevails over all the other excitation sources. If the dominant seismic excitation is measured, the identification problem belongs to the MIMO class for Linear Time-Invariant (LTI) systems described by the equations

$$\mathbf{x}_{k+1} = \mathbf{A}\mathbf{x}_k + \mathbf{B}\mathbf{u}_k + \mathbf{w}_k \tag{13}$$

$$\mathbf{y}_k = \mathbf{C}\mathbf{x}_k + \mathbf{D}\mathbf{u}_k + \mathbf{v}_k \tag{14}$$

where $\mathbf{u}_k \in \Re^m$ is a vector of m measured inputs at the time step k, $\mathbf{y}_k \in \Re^l$ is a vector of l measured outputs at time step k, and $\mathbf{x}_k \in \Re^n$ is an n-dimensional unknown discrete state vector. The two stochastic terms $\mathbf{w}_k \in \Re^n$ and $\mathbf{v}_k \in \Re^l$ are assumed as uncorrelated Gaussian zero-mean white noise processes, with unknown covariance matrix

$$\mathbf{E}\left[\begin{pmatrix}\mathbf{w}_p \\ \mathbf{v}_p\end{pmatrix}\begin{pmatrix}\mathbf{w}_q^T & \mathbf{v}_q^T\end{pmatrix}\right] = \begin{pmatrix}\mathbf{Q} & \mathbf{S} \\ \mathbf{S}^T & \mathbf{R}\end{pmatrix}\delta_{pq} \tag{15}$$

where δ_{pq} is a Kronecher delta. The identification procedure aims to solve the following inverse problem: "given the measured input sequence $\mathbf{U}_i$ and the output sequence $\mathbf{Y}_i$ defined as $\mathbf{U}_i = [\mathbf{u}_i, \mathbf{u}_{i+1}, \ldots \mathbf{u}_{i+j-1}] \in \Re^{m\times j}$ and $\mathbf{Y}_i = [\mathbf{y}_i, \mathbf{y}_{i+1}, \ldots \mathbf{y}_{i+j-1}] \in \Re^{l\times j}$ with $j \to \infty$, determine the unknown system matrices $\mathbf{A} \in \Re^{n\times n}$, $\mathbf{B} \in \Re^{n\times m}$, $\mathbf{C} \in \Re^{l\times n}$, $\mathbf{D} \in \Re^{l\times m}$ and the matrices $\mathbf{Q} \in \Re^{n\times n}$, $\mathbf{S} \in \Re^{n\times l}$, $\mathbf{R} \in \Re^{l\times l}$".

4.3 Inverse problem: subspace state-space system identification

In the above-mentioned framework, Subspace State-Space System identification (4SID) methods are considered to possess certain specific features to deal with noisy data acquired during rapid dynamic testing [14, 17, 19] or under seismic induced vibrations [36].

In the general case of input–output 4SID methods, a geometric interpretation of each specific step of the procedures can be given. Indeed, the measurements of the system input $\mathbf{U}_i$ and output $\mathbf{Y}_i$ are used to define two subspaces spanned by the input sequence $\mathbf{U}$ and the colored noise output sequence $\mathbf{Y}_i^s$, respectively, and one subspace spanned by the joint null space of the input and the colored noise output $\left\{\mathbf{U}_i^\perp, \mathbf{Y}_i^{s\perp}\right\}$. The leading idea of 4SID is the estimation of the product $\mathbf{\Gamma}_i\mathbf{X}_i$ of the well-known extended observability matrix $\mathbf{\Gamma}_i$, and the state space sequence $\mathbf{X}_i$ which are aligned to the null space $\left\{\mathbf{U}_i^\perp, \mathbf{Y}_i^{s\perp}\right\}$.

In view of the use of 4SID methods for the evaluation of the eigenproperties of several stochastic discrete state space models, characterized by increasing order r, the main aspects of the identification processes are summarized in the following.

The leading idea at the base of 4SID methods is that the unknown state-space matrices, defining the state-system in Eqs. (13) and (14), which can be combined leading to

$$\begin{bmatrix}\mathbf{X}_{i+1} \\ \mathbf{Y}_{i|i}\end{bmatrix} = \begin{bmatrix}\mathbf{A} \\ \mathbf{C}\end{bmatrix}\mathbf{X}_i + \begin{bmatrix}\mathbf{B} \\ \mathbf{D}\end{bmatrix}\mathbf{U}_{i|i} + \begin{bmatrix}\mathbf{W} \\ \mathbf{V}\end{bmatrix} \tag{16}$$

where W and V are, respectively, the matrices of the two stochastic terms w_k and v_k, are estimated by a least square solution on the basis of the two sequence estimates $(\hat{\mathbf{X}}_{i+1}, \hat{\mathbf{X}}_i)$ as

$$\begin{bmatrix}\hat{\mathbf{A}} & \hat{\mathbf{B}} \\ \hat{\mathbf{C}} & \hat{\mathbf{D}}\end{bmatrix} = \begin{bmatrix}\hat{\mathbf{X}}_{i+1} \\ \mathbf{Y}_{i|i}\end{bmatrix}\begin{bmatrix}\hat{\mathbf{X}}_i \\ \mathbf{U}_{i|i}\end{bmatrix}^\dagger \tag{17}$$

where the apex † indicates the pseudo-inverse and the input and output sequences are gathered in block Hankel matrices (a Hankel matrix is a matrix where each anti-diagonal consists of the repetition of the same element) for which the subscripts report the subscript of the first and last element in the first column of the block Hankel matrix. As a result, 4SID algorithms seek the identification of the state-space matrices through the estimation of the state sequence using the measured input and output sequences, if both are available, or only the output one.

As far as even in seismic monitoring the acceleration at the base can either be measured or not, different procedures can be adopted. In the case of unknown base accelerations, SSI-COV or SSI-DATA are useful procedures, demonstrated equivalent in some sense [15], which allow a suited reduction of the matrix dimensions by introducing the idea of reference sensors [14]. When the base accelerations are available, they can be considered deterministic system inputs, and different selected sensors can be considered as the reference ones, in reference-based combined deterministic-stochastic subspace identification methods (CSI/ref) [17]. All the above-mentioned methods are based on a main theorem of subspace identification that indicates how the combined deterministic-stochastic Kalman filter state sequences can be directly extracted from the input–output sequences and even from the output sequence only.

For example, the CSI/ref algorithm, relevant for seismic monitoring, starts with the development of a Kalman filter (governed by the matrix K_k) that makes use of the reference outputs $\mathbf{y}_k^{\text{ref}}$, a subgroup selected by the user from the complete set of outputs, and goes on with the decomposition of the state in its deterministic and stochastic components (see [17]) leading to the state estimation

$$\begin{aligned}\hat{\mathbf{x}}_{k+1} &= \mathbf{A}\hat{\mathbf{x}}_k + \mathbf{B}\mathbf{u}_k + \mathbf{K}_k(\mathbf{y}_k^{\text{ref}} - \mathbf{C}^{\text{ref}}\hat{\mathbf{x}}_k - \mathbf{D}^{\text{ref}}\mathbf{u}_k) \\ &= \mathbf{A}\hat{\mathbf{x}}_k + \mathbf{B}\mathbf{g}_k + \mathbf{E}\mathbf{f}_k + \mathbf{K}_k\mathbf{e}_k^{\text{ref}}\end{aligned} \tag{18}$$

in which $\mathbf{e}_k^{\text{ref}}$ is called the *reference-based forward innovation*. Then, assuming that only the seismic excitation is measured, in order to proceed with the identification of the system matrices **A**, **B**, **C** and **D**, and of the noise covariance matrices **Q**, **R** and **S**, the measured output and input are grouped into the block Hankel matrices

$$\mathbf{Y}_{0|2i-1} = \frac{1}{\sqrt{j}}\begin{bmatrix} \mathbf{y}_0^{\text{ref}} & \mathbf{y}_1^{\text{ref}} & \mathbf{y}_2^{\text{ref}} & \cdots & \mathbf{y}_{j-1}^{\text{ref}} \\ \mathbf{y}_1^{\text{ref}} & \mathbf{y}_2^{\text{ref}} & \mathbf{y}_3^{\text{ref}} & \cdots & \mathbf{y}_j^{\text{ref}} \\ \cdots & \cdots & \cdots & \cdots & \cdots \\ \mathbf{y}_{i-1}^{\text{ref}} & \mathbf{y}_i^{\text{ref}} & \mathbf{y}_{i+1}^{\text{ref}} & \cdots & \mathbf{y}_{i+j-2}^{\text{ref}} \\ \mathbf{y}_i & \mathbf{y}_{i+1} & \mathbf{y}_{i+2} & \cdots & \mathbf{y}_{i+j-1} \\ \mathbf{y}_{i+1} & \mathbf{y}_{i+2} & \mathbf{y}_{i+3} & \cdots & \mathbf{y}_{i+j} \\ \cdots & \cdots & \cdots & \cdots & \cdots \\ \mathbf{y}_{2i-1} & \mathbf{y}_{2i} & \mathbf{y}_{2i+1} & \cdots & \mathbf{y}_{2i+j-2} \end{bmatrix} = \begin{bmatrix} \mathbf{Y}_p^{\text{ref}} \\ \mathbf{Y}_f \end{bmatrix}$$

$$\mathbf{U}_{0|2i-1} = \frac{1}{\sqrt{j}}\begin{bmatrix} \mathbf{u}_0 & \mathbf{u}_1 & \mathbf{u}_2 & \cdots & \mathbf{u}_{j-1} \\ \mathbf{u}_1 & \mathbf{u}_2 & \mathbf{u}_3 & \cdots & \mathbf{u}_j \\ \cdots & \cdots & \cdots & \cdots & \cdots \\ \mathbf{u}_{i-1} & \mathbf{u}_i & \mathbf{u}_{i+1} & \cdots & \mathbf{u}_{i+j-2} \\ \mathbf{u}_i & \mathbf{u}_{i+1} & \mathbf{u}_{i+2} & \cdots & \mathbf{u}_{i+j-1} \\ \mathbf{u}_{i+1} & \mathbf{u}_{i+2} & \mathbf{u}_{i+3} & \cdots & \mathbf{u}_{i+j} \\ \cdots & \cdots & \cdots & \cdots & \cdots \\ \mathbf{u}_{2i-1} & \mathbf{u}_{2i} & \mathbf{u}_{2i+1} & \cdots & \mathbf{u}_{2i+j-2} \end{bmatrix} = \begin{bmatrix} \mathbf{U}_p \\ \mathbf{U}_f \end{bmatrix} \tag{19}$$

where the upper $\mathbf{Y}_p^{\text{ref}}$, $\mathbf{U}_p$ and lower half $\mathbf{Y}_f$, $\mathbf{U}_f$ are known as the *past* and *future* reference output and input submatrices, respectively. The key step of the method is the oblique projection [12] of the row space of $\mathbf{Y}_f$ onto the joint row space of $\mathbf{U}_p$ and $\mathbf{Y}_p^{\text{ref}}$ in the direction of the row space of $\mathbf{U}_f$ giving the projection matrix

$$\mathbf{\Theta}_i = \mathbf{Y}_f / \mathbf{U}_f \begin{bmatrix} \mathbf{U}_p \\ \mathbf{Y}_p^{\text{ref}} \end{bmatrix} \tag{20}$$

Based on the main theorem of subspace identification which states that, if the process noise $\mathbf{w}_k$ and the measurement noise $\mathbf{v}_k$ are uncorrelated with the deterministic input $\mathbf{u}_k$ and if $\lim_{j\to\infty} \mathbf{U}_{0|2i-1}\mathbf{U}_{0|2i-1}^T$ has full rank, it can be proved that

$$\text{a.s.} \quad \lim_{j\to\infty} \mathbf{\Theta}_i = \lim_{j\to\infty} \mathbf{\Gamma}_i \hat{\mathbf{X}}_i \tag{21}$$

where the almost-sure limit (a.s.lim) [17] indicates that the expression is strongly consistent and $\mathbf{\Gamma}_i$ is the extended observability matrix, defined as $\Gamma_i = [\mathbf{C}\,\mathbf{CA}\,\mathbf{CA}^2 \ldots \mathbf{CA}^{i-1}]^T$ and $\hat{\mathbf{X}}_i$ is the sequence of reference-based Kalman filter states $\hat{\mathbf{X}}_i = [\hat{\mathbf{x}}_i \hat{\mathbf{x}}_{i+1} \ldots \hat{\mathbf{x}}_{i+j-2} \hat{\mathbf{x}}_{i+j-1}]^T$, with the initial value $\hat{\mathbf{X}}_0 = \mathbf{X}_0^d / \mathbf{X}_{0|2i-1}$.

The estimation of the two matrices $\mathbf{\Gamma}_i$ and $\hat{\mathbf{X}}_i$ is based on the SVD of the projection matrix $\mathbf{\Theta}_i = \mathbf{U}_1\mathbf{\Sigma}_1\mathbf{V}_1^T$ so that

$$\mathbf{\Gamma}_i = \mathbf{U}_1\mathbf{\Sigma}_1^{1/2}, \quad \hat{\mathbf{X}}_i = \mathbf{\Sigma}_1^{1/2}\mathbf{V}_1^T \tag{22}$$

Once the matrices $\mathbf{\Gamma}_i$ and $\hat{\mathbf{X}}_i$ are estimated, together with $\hat{\mathbf{X}}_{i+1}$, simply iterating at $i + 1$, the extraction of the state matrices based on a least-squares solution of Eq. (17) and the evaluation of the system eigenproperties therefrom, are achievable [10, 12, 14, 15, 17].

According to the procedure described above, the size of the Hankel matrices $\mathbf{Y}_{0|2i-1}$ and $\mathbf{U}_{0|2i-1}$, and thus also the size of the projection matrix $\mathbf{\Theta}_i$ determines the order of the identified model. Normally, for actual civil engineering structures it is almost impossible to predict the order of the model that better fits the experimental data, giving a realistic description of the structural dynamic behavior. Therefore, it could be convenient to iterate the modal parameter estimation for several models with decreasing order, fixing a conservative high-order starting point, and continuing until an optimal synthesis is achieved, according to a user-defined balanced criterion of sufficient representativeness and minimal order. The identified modal frequencies can be simultaneously represented in the so-called stabilization diagram to evidence those maintaining similar values (stability) for increasing order models. Stable frequencies, with the associated modes, tend to be recognized as belonging to the natural spectrum of the

structure, while the others can be related to numerical modes, able to describe the measurement noise.

5 Data collection and analysis

The acquisition of reliable data from a monitoring system based on a WSN requires a series of operations which must be conducted with particular care and attention. In the present section the experiences of data acquisition and analysis during the development of the permanent monitoring system at the Basilica di Collemaggio are summarized. In particular, the work has been conducted in three main phases: calibration in the lab environment, initial on-site validation tests, and on-going network management and enhancement.

The analysis of the data collected by the monitoring system was anticipated by a preliminary phase, devoted to comparing the performance of each single wireless node with a reference wired sensor in a controlled laboratory environment.

The validation phase of the monitoring system had two main goals: characterization of the performance of each wireless sensor node (determination of the scale and offset factors for each axis of each sensor node) and analysis of the structural dynamic response by means of the measured acceleration signals.

Several numerical and experimental studies were conducted on the Basilica before and after the 2009 L'Aquila earthquake. The available data from the previous on-site dynamic campaign were used to develop finite element models of the Basilica; these models were able to reproduce the main modal identified characteristics and consequently aided investigation into the causes of the partial collapse of the transept [18].

Starting from this knowledge, the installation of the WSN through 15 sensors with tri-axial accelerometers was completed in 3 days on June 20–22, 2011; since that date, both seismic and environmental-induced vibrations on masonry elements have been measurable. The first acquisitions of the acceleration response of the Basilica under ambient excitations show that the masonry structure, supported by a series of scaffolding systems, experienced very low vibration amplitudes. In this case, the acquired measurements generally evidence a very low signal-to-noise ratio, making practically impossible the extraction of a modal signature from the data. In practice, the normal environmental sources of excitation coming either from traffic (located far away from the Basilica), microtremors at the foundation, or wind pressure on the structure are not able to generate a sufficient level of acceleration amplitudes. Indeed, the modal acceleration components contributing to the overall signal are distributed among several modes in monumental structures such as the Basilica of Collemaggio. Such contributions include local modes, which may involve a few macro-elements or portions of them, lying in a wide frequency range including high-frequency components [19, 35]. Therefore, participating in the structural response to seismic- or even wind-induced loadings are a variety of modes which scatter the entering energy across a wide frequency spectrum. Consequently, a significant input energy is necessary to excite even the main modal components sufficiently to measure signals which overcome the noise level of the MEMS accelerometer installed in the Imote2 sensor, with the specific features given in Table 1, and consequently to verify the ability of the accelerometer monitoring system.

During the months following the installation, the monitoring system was continuously enhanced to the point of complete and automated operation in sensing seismically-induced vibrations. To date, several events with relevant dynamic effects have been observed and measured, among them structural accelerations induced by far- and near-field earthquakes. The information from the cases most significant for identification purposes has been reported in Table 2. The first column lists the location of the earthquake epicenter and the second column provides an estimation of the approximate distance from the epicenter. Date, time and earthquake magnitude follow. The last two columns show two major significant values coming from the monitoring system: the peak response acceleration amplitude registered by the WSN, and the group of sensors in current operation during the shake. Recorded structural responses show prevailing out-of-plane oscillations of the nave walls.

Low magnitude events furnish a sufficient level of energy to overcome the noise threshold of the monitoring system, allowing the recording of acceleration data characterized by a sufficient structural signature.

Consequently, spectral analysis has been used to extract preliminary information from the recorded data, clearly evidencing the change in the main natural frequencies with respect to the values measured in the pre-earthquake configuration.

Figure 4 reports the power spectral densities (PSDs) of the response measured at the sensor nodes located in one of the internal nave walls. Looking at the corresponding plots disposed row-wise, the presence of different amplitudes in the range between 2.5 and 4.5 Hz is evident. The reason for this difference may be attributed to the different nature of the seismic inputs. In particular, the left and the right columns refer to a seismic event having a very long (E3 in Table 2, more or less 300 km) or very short (E6 in Table 2, about 10 km) epicentral distance from the Basilica, respectively. In far-field E3 event, the low energy of the earthquake, probably contained in a narrow range of

Table 2 Main seismic events recorded by the WSN at the Basilica S. Maria di Collemaggio

	Earthquake/epicenter	D	Date	Time (UTC)	*M*	PRA (mm/s^2)	Group
E1	Main Emilia/Finale Emilia	F	20/05/2012	2:03 AM	5.9	70.4	I
E2	After Emilia/Vigarano	F	20/05/2012	1:18 PM	5.1	17.9	II
E3	After Emila/Cervia-Ravenna	F	06/06/2012	6:08 AM	4.5	10.9	I
E4	L'Aquila/Scoppito	N	14/10/2012	4:32 PM	2.8	71.7	II
E5	L'Aquila/Pizzoli-Scoppito	N	30/10/2012	2:52 AM	3.6	72.7	II
E6	L'Aquila/Pizzoli	N	16/11/2012	3:37 AM	3.2	83.2	I
E7	L'Aquila/Val di Sangro	N	14/02/2014	8:51 PM	2.9	26.2 (60.4)	I
E8	L'Aquila/Valle dell'Aterno	N	04/09/2014	3:55 PM	2.1	18.8	I

D distance of the epicenter (*F* far, *N* near), *M* magnitude. () relative to the node 37 in global *X*-direction

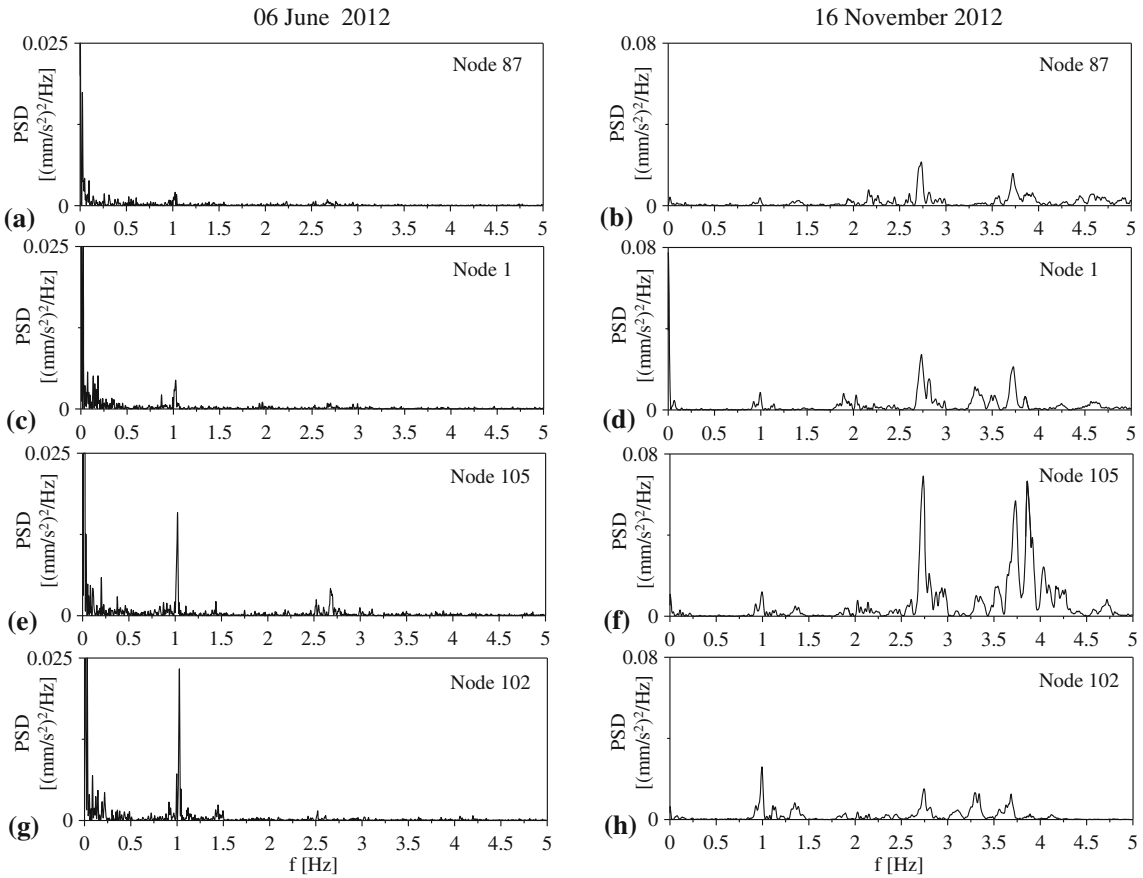

Fig. 4 Power spectral density of the accelerations acquired during the events of 06 June 2012 (**a**, **c**, **e**, **g** E3 in the Table 2) and of 16 November 2012 (**b**, **d**, **f**, **h** E6 in the Table 2). Nodes belonging to the Group I. Acceleration in *Y*-direction (transversal direction of the inner walls)

frequencies due to a filtering process obtained for the distance of the epicenter, apparently applied a sort of small impulse, as evident in the PSDs where the response peaks at 1 Hz can be associated with structural modes. On the contrary, in the near-field E6 event the high energy was spread in a wide range of frequencies, inducing the interaction between the structure and the safety system (involving probably and mainly the wall-cable interaction), but also amplifying the modal components belonging to higher modes.

In particular, focusing attention on event E6 of Table 2, in which the highest response peak acceleration was recorded, it is possible to evidence firstly the main features of the recorded acceleration at the base (sensor 99 in Fig. 2). Indeed, Fig. 5a shows the planar trajectory of the recorded accelerations at the base and Fig. 5b–d reports

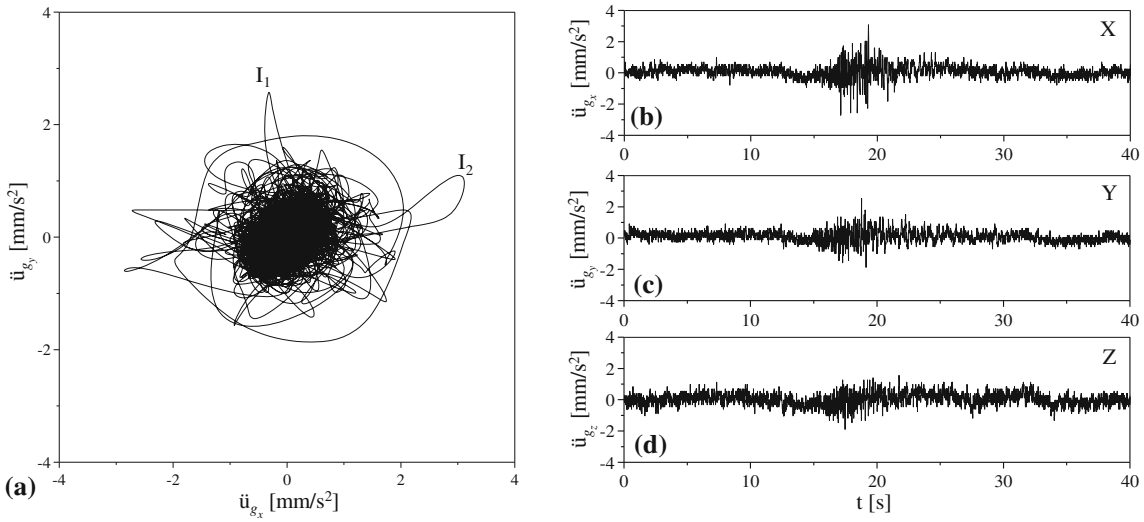

Fig. 5 Base acceleration for E6 event (sensor n. 99): **a** acceleration trajectory in the *x*–*y* plane, **b–d** time histories of the acceleration components. Node belonging to the Group I

time histories of the three acceleration components. The trajectory of the signal evidences a slight polarization in the longitudinal direction of the Basilica (*x*-axis), showing in any case the presence of two main impulses, I1 and I2, the first one mainly in the longitudinal direction, while the second one is in the transversal direction.

The modal frequency signature is clearly visible in the E6 event measurements due to a relatively high signal-to-noise ratio reached by the seismic induced-vibrations.

Indeed, Fig. 6a–c show PSDs in the range (0.5–5 Hz) of the three component acceleration signals recorded on the nave wall visible in section F–F in Fig. 2, while Fig. 6d–f evidence the frequency content of the three base acceleration components recorded at the 99-node and depicted in Fig. 5.

In particular, in this case, even if the base acceleration components (at the floor inside the church) possess a series of peaks in their own spectrum due to the interaction with the church structures (the 99-node is positioned on the base of a column and not directly on the ground), a clear signature in the frequency content of the PSDs of the two observed points (105- and 102-nodes) is evident. Peaks at low frequency in the PSD function of both selected transversal components are clearly visible in Fig. 6b (see vertical lines at 0.974, 1.393, 1.912 Hz). However, the high amplitudes of these peaks compared with the longitudinal and vertical components (Fig. 6a, c) remains relatively low with respect to the amplitudes of the peaks at the higher frequencies (in the range 2–3 Hz), probably due to large vibrations in the wall induced by tendon oscillations.

However, a different earthquake event (E2 in Table 2, epicentral distance of more or less 300 km) confirms that the first resonant natural frequency associated to modes involving a transversal behavior of the four nave walls connected at the top by the roof is around 1 Hz. During this event, in which the epicenter was far-field, sensors belonging to group II were operating. PSDs of the acquired signals are presented in Fig. 7a, c, e, d. In these plots are reported only the peak amplitudes of the transversal signals that are larger than the other two components. It is clearly visible that larger components of the signal are around the frequency of 1 Hz. This evidences that at the 152-node the far-field earthquake, which probably had a large horizontal component relative to the vertical one and a low-frequency content, excited the first mode of the structure more than in the near-field occurrences (see the highest peak in Fig. 7b which appears at the frequency value of 0.967 Hz which is lower than the peak contained in the signal of the symmetric 105-node during the E6 events, where it was at 0.974 Hz as evidenced by the dotted vertical line).

The complex dependence of the frequency-domain response on the earthquake epicenter, and consequently on the type of induced seismic motion at the base of the Basilica, can be also observed comparing the PSDs of the signals acquired by the sensor belonging to group II in the E2 and E5 events. Indeed, in Fig. 7 the frequency signature in the PSDs of the signals acquired during the near-field earthquake appears quite different from what is observed in the previous case. Also in this case, as well as observed in the case of the node belonging to the group I (Fig. 2), a near-fault earthquake (E5), having an higher energy spread in a wide range of frequencies, produces PDSs with different peaks scattered in the whole range of frequencies between 1 and 5 Hz (Fig. 7b, d, f, h). Similar to the behavior observed in the E6 event, a spread of energy around the range frequency, included between 2.5 and

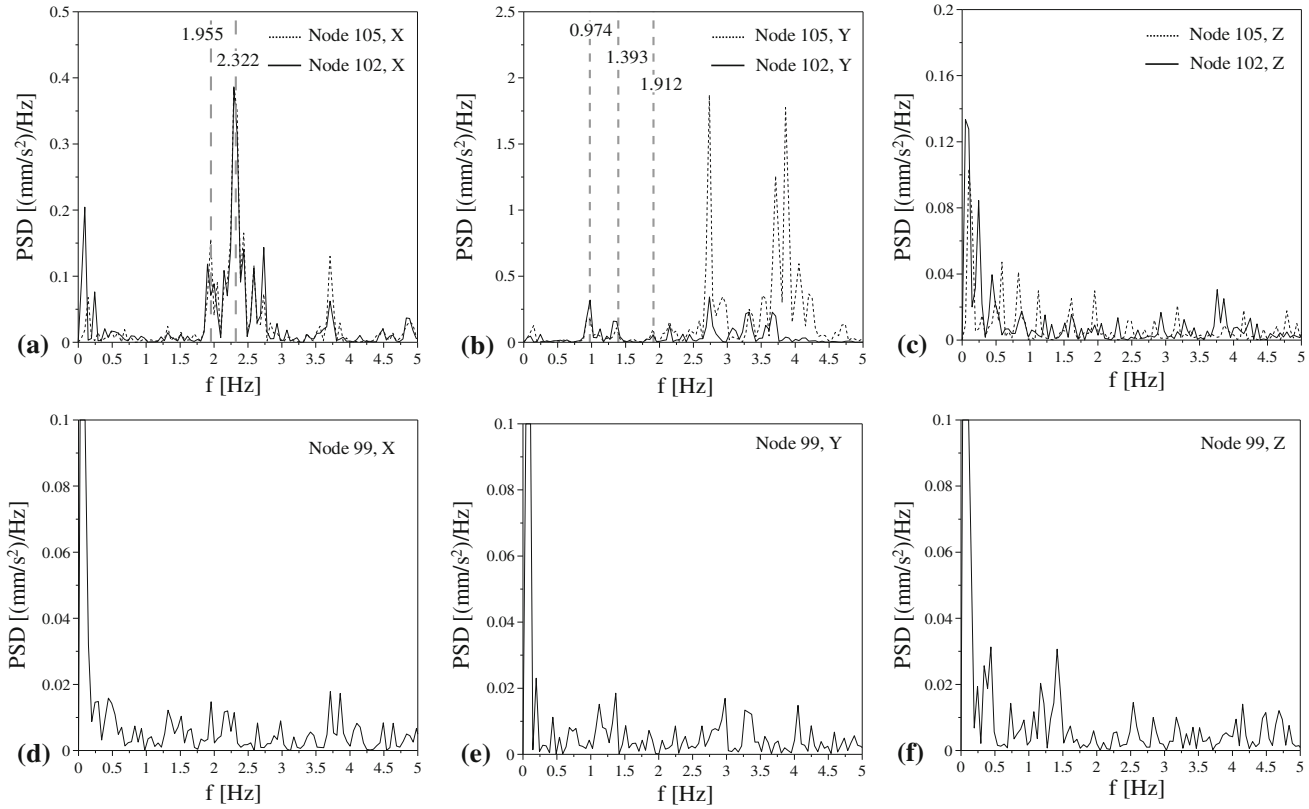

Fig. 6 Power spectral density of the accelerations acquired during the earthquake of 16 November 2012 (E6 Table 2). Nodes belonging to the Group I

4.5 Hz, probably due to the tendon vibration, can also be observed in the E5 event.

Figure 8 describes the information obtained by the sensors mounted on the facade of the Basilica. In particular, the recorded acceleration during the E7 earthquake event at the 37-node over the tower (see section E–E on Fig. 2) shows that in the longitudinal *x*-direction of the church (transversal for the facade) it is still possible to recognize the frequency signature, due probably to the tendons oscillations, which has been estimated around 2.5 Hz. It is necessary to highlight that such a peak amplitude is present in the accelerations in the longitudinal *x*-direction components recorded on the sensors positioned on the nave walls. This behavior clearly shows that the longitudinal oscillations of the central nave induce transversal oscillations of the façade, which are not prevented by the scaffolding system inserted in the arches of the central wall to stiffen their in-plane behavior. In this range, previous dynamic testing on the facade has shown a series of local modes, which involve deformation of the upper free-standing part of the façade; the façade possesses its own out-of-plane stiffness, but because of its height is prone to oscillate due to the amplification of the substructures. In the case of the E7 event, the registration of the peak acceleration transversally to the facade at 60.4 mm/s^2 permits calculating an amplification ratio of 2.3 with respect to the maximum peak acceleration recorded on the nave walls (26.2 mm/s^2).

6 SSI with seismic-response data

The system identification step plays a crucial role in structural monitoring because the identified system model determines the quality and number of the modal parameters that can be derived from it. In this regard, an SSI based-procedure has here been used to derive a reliable parametric model, from which the modal parameters have then been determined under a different hypothesis. Questions regarding the legitimacy of using SSI procedures to identify an LTI system in the case of seismic induced vibrations are relevant. The ability of SSI procedures to handle large amounts of noisy data has made these techniques appealing in the treatment of seismic monitoring data. The use of combined input–output (or output-only) SSI procedures has been recently discussed with regard to numerical simulations of the excitation of a tower's structural supports due to passage of trucks on a traffic plateau, the excitations

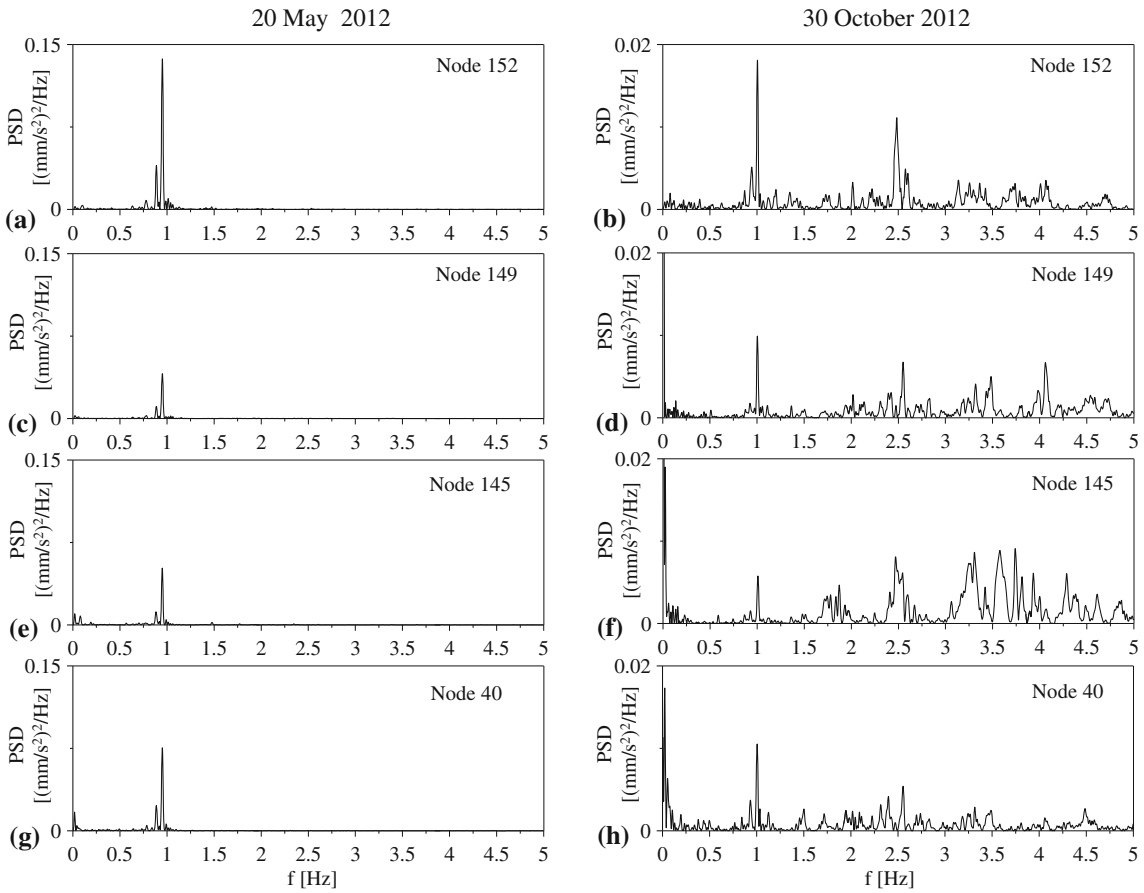

Fig. 7 Power spectral density of the accelerations acquired during the events of 20 May 2012 (**a**, **c**, **e**, **g** E2 in the Table 2) and 30 October 2012 (**b**, **d**, **f**, **h** E5 in the Table 2). Nodes belonging to the Group II. Acceleration in *Y*-direction (transversal direction of the inner walls)

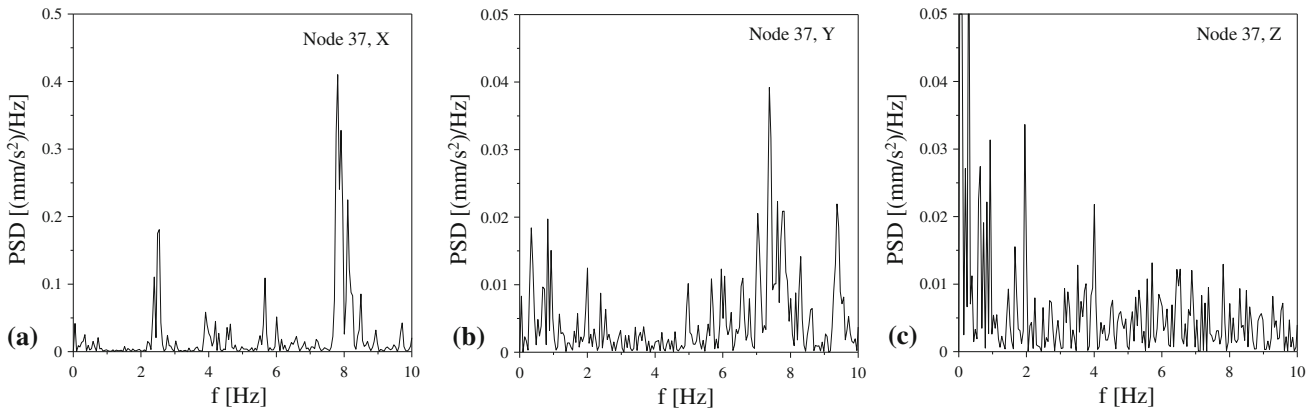

Fig. 8 Power spectral density of the accelerations acquired on the facade during E7 seismic event. Node belonging to the Group I

being considered as a measured (or unmeasured) deterministic input [36]. Recently, the ability of an input–output state space model identified through SSI procedures has been demonstrated to reproduce well the experimental response data for El Centro and white noise excitation tests [37]. In this study, it has been shown that an opportune selection of the model order ($n = 36$) in the input–output SSI process, using the white noise test data sets, demonstrates the model's ability to reproduce the output signal for both the white noise and El Centro tests. Massive use of SSI for LTI systems has been recently performed on data coming from long-term seismic response monitoring of modern infrastructures [38], while in the case of strong earthquakes both a time-invariant system using a moving

window and a time-variant (TV) system using a recursive least square have been used to estimate LTI and LTV models able to reproduce the peculiar seismic behavior of isolated structures [39], while data-driven nonlinear time variant (NTV) mathematical models have been identified for response prediction and damping estimation of long-span monitored bridges subjected to strong earthquakes [40].

In the present case, on the basis of the research indicating the robustness of 4SID algorithms with respect to nonstationary inputs (white noise sequences with time varying covariance) [15, 41], a tentative attempt to demonstrate the ability of SSI procedures to identify a robust LTI system with respect to the input characteristics of small earthquakes through long-term seismic monitoring data has been pursued, despite almost prohibitive uncertainties and "real world" complications.

The identification of several parametric dynamic models has been performed considering the E6 event, in which the highest peak acceleration amplitudes have been registered, as a reference case. Both SSI-COV and SSI-DATA procedures have been used; in particular, in the second case the concepts of both reference-based and combined-subspace identification have been applied to extract valuable information regarding the robustness of the modal parameters extracted from noisy measurements. Figure 9 shows the results of the identification process in the form of stabilization diagrams. The bias and variance errors of this stabilization diagrams, based on the experience observed in [42], have been removed using in opportune way the so-called stabilization criteria (such as the expected proprieties of mode shapes or the expected damping ratio range). SSI-COV was first used with a set of four acceleration measurements transversal to the nave wall, visible in section F–F of Fig. 2. The method has permitted identification of a series of parametric models described by Eqs. (11)–(12) with increasing system dimension (order of the identified system). Hence, eigenproperties of the identified system have been extracted for each system increasing its dimension. In Fig. 9, the lower eigenfrequencies are plotted versus the model order, identified from the recorded measurements during the E6 event. Increasing the order of the identified system, four other eigenfrequencies appear with the increase of the model order (up to 200). Using the measurements of sensor 87 (see Fig. 9b) as a reference signal, the stabilization diagram is cleaned up, and the errors in the identification of the lower eigenfrequencies due to the increasing of the model order, probably due to the noise in the data, are minimized showing small differences in the identification frequencies increasing the model order.

If the longitudinal accelerations in the x-direction are used together with the transversal direction, the modification introduced in the stabilization diagram for the first natural frequencies is negligible as is evident by comparing Fig. 9c, d with Fig. 9a, b. It should be noted that the use of the longitudinal measurements actually makes the identification process more robust.

In order to evaluate the influence of the selected reference point in the eigenfrequency estimation, different sensors have been selected to serve as reference ones determining different analyzed cases. The results obtained for the first three frequencies are summarized in Table 3.

The results show a slight dependence of the frequency values on the selected reference sensor. In all procedures the standard deviations σ of the identified frequencies

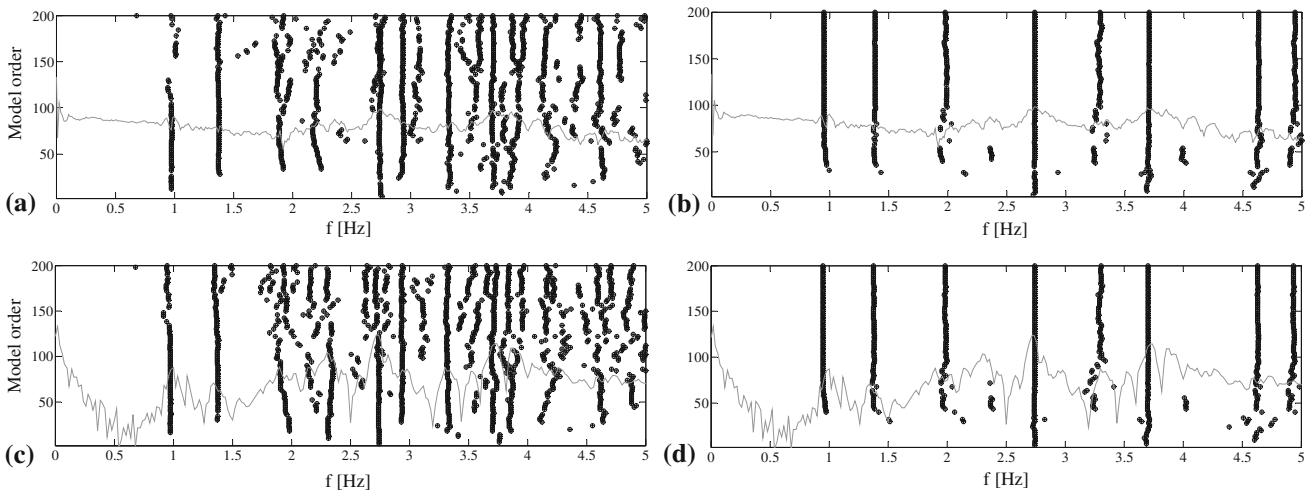

Fig. 9 Stability diagrams obtained by using selected measurements recorded on the nodes 87, 1, 105 and 102 during the E6 event in the SSI-covariance driven procedure: only transversal accelerations: **a** all output, **b** node 87 as reference; transversal and longitudinal accelerations: **c** all output, **d** node 87 as reference

Table 3 First three identified frequencies during the E6 seismic event in the group I sensor nodes

	SSI-COV			SSI-DATA			CSI		
	Frequency (Hz)			Frequency (Hz)			Frequency (Hz)		
	Mode 1	Mode 2	Mode 3	Mode 1	Mode 2	Mode 3	Mode 1	Mode 2	Mode 3
All	0.991	1.389	1.936	0.983	1.375	1.917	0.983	1.385	1.915
Ref 87	0.977	1.379	1.907	0.995	–	–	0.971	1.406	1.921
Ref 1	0.971	1.368	1.891	0.920	1.374	–	0.976	1.403	1.891
Ref 105	0.985	1.359	2.014	0.920	1.350	–	0.980	1.395	1.894
Ref 102	0.976	1.386	1.845	0.999	1.363	–	0.981	1.409	1.931
Ref 87–1	1.003	1.374	1.974	0.973	1.384	1.893	0.975	1.406	1.916
Ref 1–105	1.002	1.374	1.978	0.985	1.368	1.958	0.978	1.388	1.907
Ref 105–102	–	–	1.971	0.985	1.390	1.920	0.977	1.387	1.901
μ	0.986	1.376	1.940	0.970	1.372	1.922	0.978	1.397	1.910
σ	0.012	0.010	0.052	0.030	0.012	0.023	0.004	0.009	0.013

obtained when changing the reference sensor are quite small. In SSI-COV and SSI-DATA procedures, the selection of different reference measurements evidences that the beneficial effect of using a reference signal can be completely negated by the dependence of the expected eigenfrequencies on the model order. In contrast, the CSI procedure permits identification of the first three frequencies for all cases of the reference selection.

Further investigations were devoted to the dependence of the first three identified modal frequencies on the type of seismic excitation. In this regard, averaging the identified frequencies with respect to all possible selections of the reference sensor and considering different seismic excitations permitted the evaluation of the influence of both noise and excitation in the eigenfrequency identification. Indeed, the dependence with respect to three different seismic events of the frequency estimation evaluated by SSI-COV (Fig. 10a), SSI-DATA (Fig. 10b) and CSI (Fig. 10c) is summarized through mean μ and standard deviation σ values obtained also for the E1 and E3 events, with the same procedure used for the E6 event, as summarized in Table 3. The graph shows that, averaging the results obtained for the three seismic events, the deviations from the average are contained within small values; therefore, the mean value of the identified frequencies, varying with the reference sensor, is insensible to the nature of the experienced earthquake, whether near- (E6) or far-field (E1, E3), probably due to the small intensity of the energy involved. In particular, in the case of the E6 event, the use of measurements at the base as a known input has permitted identification of the frequencies through the CSI procedure. In this case (see Fig. 10c), the mean value of the identified frequencies for the E6 event appears practically coincident with the average value obtained considering different events, showing how the use of the input through the CSI procedure reduces the level of the inherent uncertainties. Looking at the modal shapes associated to the average values of the natural frequencies, obtained by averaging the set of all identified modes, a reasonable deflection of the central nave wall is recognized for the first three modes (Fig. 11). The first modal shape evidences a sort of cantilever deformation of the nave wall, which is restrained at the end by the strong in-plane stiffness of the facade (Fig. 11a).

Coherent with this result, the second and third modes have shapes in which the occurrence of positive and negative displacements is observed (Fig. 11b, c). Figure 12 shows the identified values of the model damping pursued by the SSI covariance-driven procedure. The damping for each model is reported for the first three modes, associated to the lowest stable poles shown in the stability diagram in Fig. 9b. The damping values seems to be rather high (3.3 % for the first mode, 4.7 and 6.6 % for the second and third, respectively) in comparison with the recurrent values

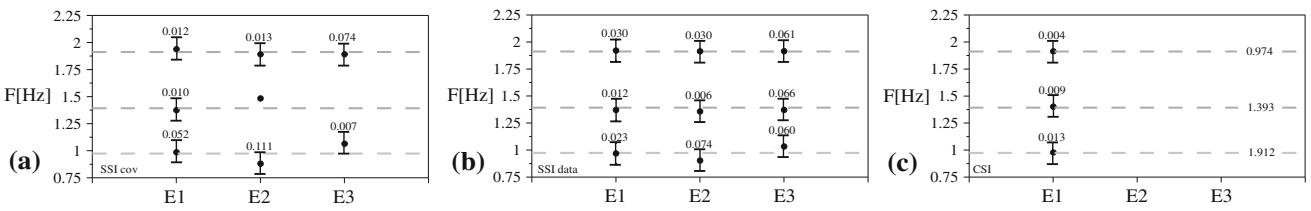

Fig. 10 Identification of the first three frequencies by means of the seismic recorded data

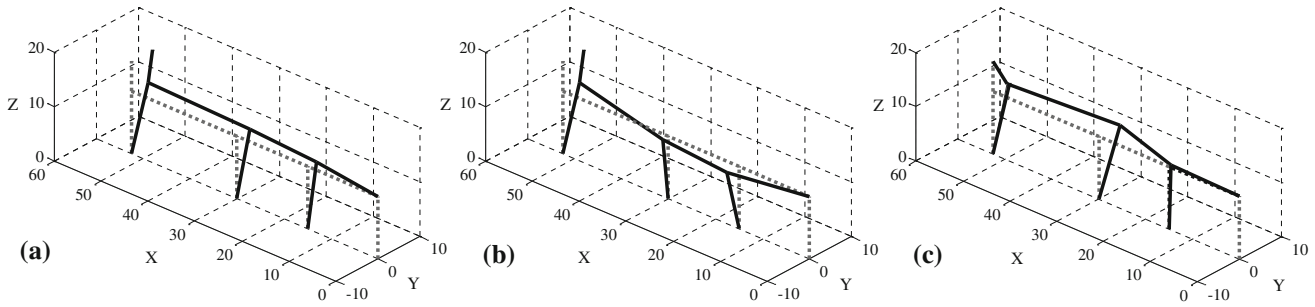

Fig. 11 First three modal shapes identified from measurements acquired by sensors (Group I) during E6 event: 3D views, **a** first mode, **b** second mode, **c** third mode

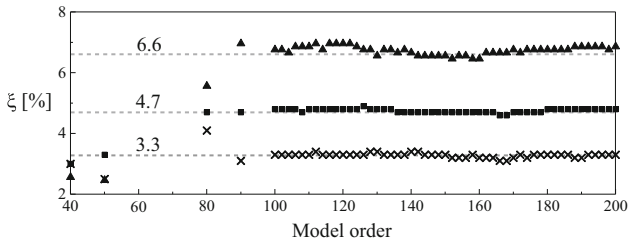

Fig. 12 Damping related to the first three modal shapes identified from measurements acquired by sensors (Group I) during E6 event

of other masonry structures. However, it is worth considering that the existing severe damage, together with the structural coupling with the provisional security systems, probably offer a non-negligible incremental contribution to the apparent modal damping of the nude masonry walls. Similar evaluations have been carried out using the measurements obtained by the group II of sensors.

Figure 13 reports the stability diagrams obtained coherently with the previous case but using the measurements acquired by the group II nodes during the E2 seismic event.

The effect of using selected reference measurements is clearly visible also in this case, comparing Fig. 13a with b. The presence of spurious modes due to the noisy data is even worse than the previous case, probably due to the use of measurements which involve both the central wall nave, opposite to the one visible in section F–F in Fig. 2, and the North external wall, which appears to be the more flexible of the two perimetral slender longitudinal walls. The contemporary use of 12 measurements, both transversal and longitudinal, permits the identification of several natural frequencies, as depicted in Fig. 13d, avoiding the influence of noise by the use of a reference node (see the enhancement with respect to Fig. 13c). The modal shapes identified using the measurements acquired by sensors belonging to group II, averaging the results obtained by the use of different reference sensors in the SSI data-driven procedure, are coherent with the previous ones obtained for Group I. This can be observed by comparing the deflection of the internal wall in Fig. 14 with the deflection of the opposite wall in Fig. 11. The simultaneous acceleration measurements acquired by sensors positioned on both internal and external walls permitted observation of the relative motion between the two walls, which motion is not restrained by the roof in the actual configuration during the experienced earthquakes, as is clearly visible in the third identified mode (Fig. 14c).

Finally, Tables 4 and 5 evidence the dependence of the first three identified frequencies on the reference sensor selected in both SSI-COV and SSI-DATA procedures in the case of the group II sensor nodes. It appears clear that using data coming in from the same event produces very close results for the different SSI-based identification processes. In contrast, the data acquired during different events leads to identified frequencies that are slightly different in each case. Such differences can be attributed to the church conditions during the seismic event or to the specific features of the induced seismic motion.

7 Finite element model updating

Structural analyses have been conducted through finite element models, allowing both the evaluation of the seismic adequacy in the pre-earthquake (undamaged) configuration [18] and the dynamical characterization of the post-earthquake (damaged) configuration, taking into account also the presence temporary scaffolding structures (Fig. 15a). The models have been implemented in SAP2000, by respecting as much as possible all the known geometric and structural properties of the building, including the openings in the walls and the imperfect parallelism between the walls of the nave. Standards triangular and isoparametric two-dimensional plate have been used to describe the masonry walls of the Basilica. The columns of the central walls have been modeled by beam elements.

Truss elements have been used to describe the wooden beams of the roof as well as the steel truss system built at

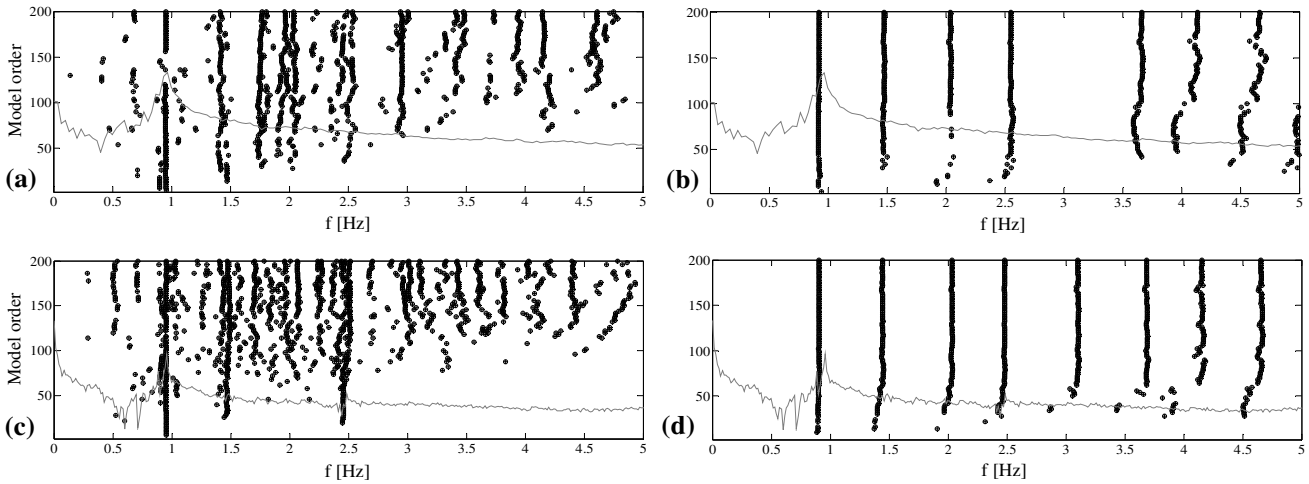

Fig. 13 Stability diagrams obtained by using selected measurements recorded on nodes 45, 40, 19, 152, 149 and 35 during the E2 event in the SSI-covariance driven procedure: only transversal accelerations: **a** all output, **b** node 152 as reference; transversal and longitudinal accelerations: **c** all output, **d** node 152 as reference

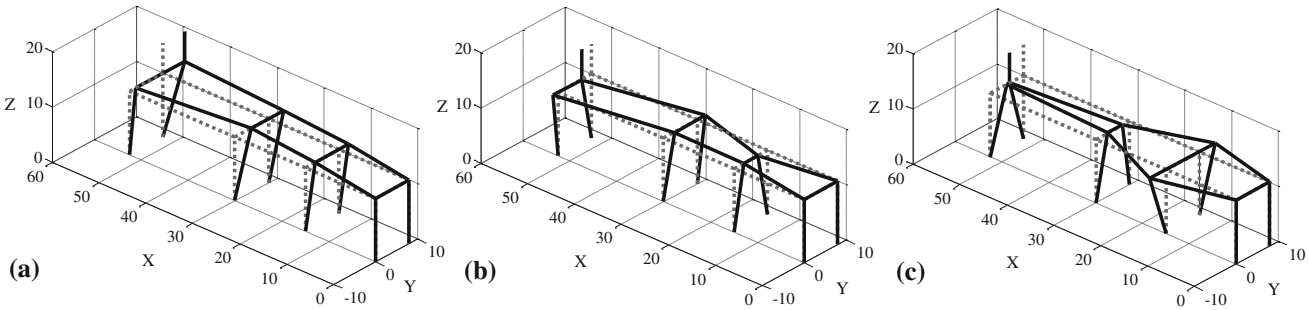

Fig. 14 First three modal shapes identified from measurements acquired by sensors (Group II) during E5 event: 3D views, **a** first mode, **b** second mode, **c** third mode

Table 4 First three identified frequencies during the E2 seismic event in the group II sensor nodes

	SSI-COV			SSI-DATA		
	Frequency (Hz)			Frequency (Hz)		
	Mode 1	Mode 2	Mode 3	Mode 1	Mode 2	Mode 3
All	0.951	1.404	1.755	0.951	1.470	1.786
Ref 145	0.948	1.471	–	0.949	1.474	–
Ref 40	0.939	–	–	0.937	–	–
Ref 19	0.949	1.473	–	0.947	1.473	–
Ref 152	0.921	1.475	2.040	0.919	1.476	2.036
Ref 149	0.920	–	1.805	0.927	–	1.808
Ref 35	0.952	1.484	–	0.952	1.482	–
μ	0.940	1.461	1.867	0.940	1.475	1.877
σ	0.013	0.029	0.124	0.012	0.004	0.113

Table 5 First three identified frequencies during the E5 seismic event in the group II sensor nodes

	SSI-COV			SSI-DATA		
	Frequency (Hz)			Frequency (Hz)		
	Mode 1	Mode 2	Mode 3	Mode 1	Mode 2	Mode 3
All	0.989	1.455	1.736	0.998	1.463	1.772
Ref 145	1.012		1.736	1.019		1.754
Ref 40	1.002	1.581	1.960	1.004	1.589	1.960
Ref 19	1.009		1.729	1.007		1.735
Ref 152	0.978		1.691	0.978		1.658
Ref 149	0.986	1.559	1.958	0.985	1.564	1.954
Ref 35	0.991		1.705	0.991		1.692
μ	0.995	1.532	1.788	0.997	1.539	1.789
σ	0.012	0.055	0.109	0.013	0.054	0.112

roof level. To take into account the nonhomogeneous material, related to the historical work operated in the church, reasonable values of the mechanical parameter (Young and Poisson moduli, mass density, etc.) have been used, initially valid on average for large areas of masonry, to be calibrated a posteriori with the use of dynamic test. In

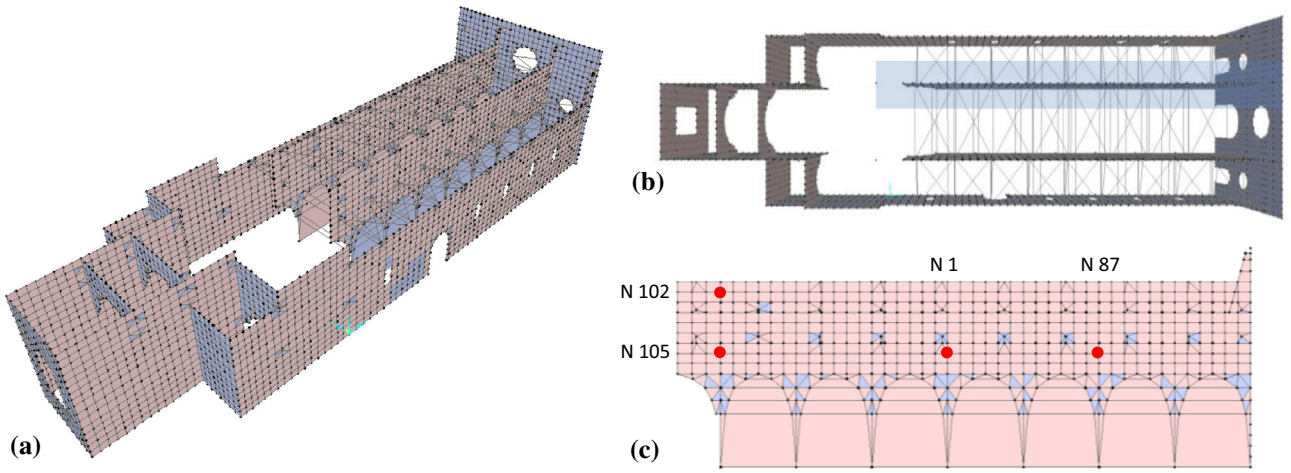

Fig. 15 Finite element model of the Basilica S. Maria di Collemaggio: **a** 3D view, **b** view from above, **c** lateral view of the inner wall highlighted in **b** with the indication of the node in which are placed the corresponding wireless sensor nodes

Table 6 Finite model updating: frequencies and MAC

Modes	Frequencies			MAC					
	Identified	Numerical	D %	Reduced			Expanded		
1	0.9780	0.9500	2.95	0.9885	0.2081	0.5100	0.9929	0.0078	0.0010
2	1.3970	1.5600	−10.45	0.4118	0.9727	0.0555	0.0079	0.9706	0.0209
3	1.9100	2.0100	−4.98	0.1327	0.0940	0.7840	0.0343	0.0240	0.9447

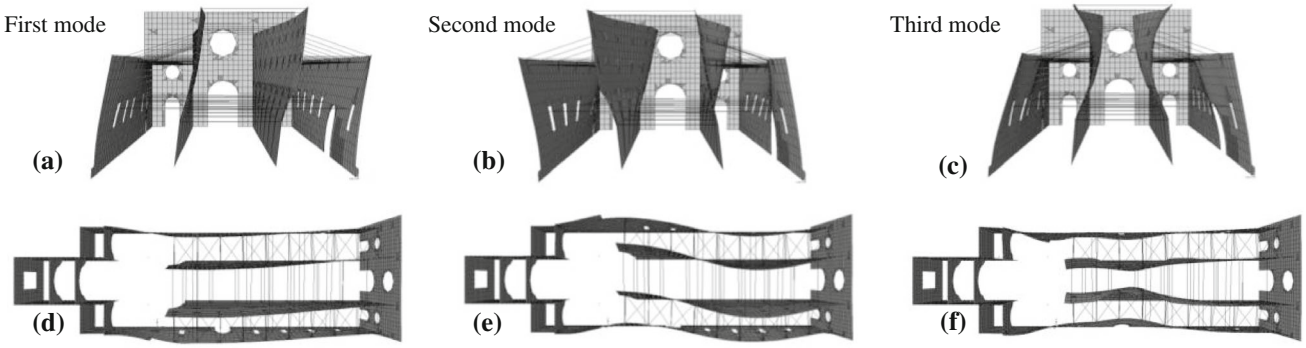

Fig. 16 First three modes of the updated model: **a–c** prospective internal view, **d–f** view from above

this phase the finite element model, representative of the pre-earthquake configuration, has been updated by minimizing the differences between the modes and frequencies identified experimentally during the dynamic test campaign performed in the year 2000 and their numerical counterparts as reported in [18].

Starting from this knowledge, a model representing the post-earthquake configuration has been developed and manual model updating has been pursed. The updating process has been conducted varying both the material characteristic and the internal connection at the roof level of the internal walls. A good agreement has been achieved in terms of both frequencies and modal shapes, compared by the Modal Assurance Criteria (MAC). Table 6 summarizes the obtained results regarding the frequency percentage difference, that does not overcome 5 % for the first and third mode and is slightly higher to the 10 % in the second mode. The lowest three modal shapes of the updated model are reported in Fig. 16, while the relative MAC values are presented in Table 6. This evaluation has been performed considering only the four modal transversal components of the numerical nodes having the same coordinate of the point in which are applied the sensor nodes (see Fig. 15c; nodes 102, 105, 1, 87) or through a

model-based expansion, described in [43], used to reconstruct complete modal shapes from the measured modal shape components.

The results show that enriching the experimental modal shapes knowledge through the finite element model permits to obtain an enhancement in the agreement between model and experimental data.

8 Conclusion

The design, deployment, management and long-term performance of a WSN has been described, with specific reference to its employment in the vibration-based seismic monitoring of a monumental structure, the Basilica S. Maria di Collemaggio in L'Aquila, Italy, after the partial transept collapse caused by the catastrophic 2009 earthquake.

The multidisciplinary experience acquired all along the multi-year monitoring project has furnished suited theoretical and applied answers to different critical issues related to the development and updating of the WSN, mainly composed of MEMS accelerometers. Key points concerned the attainment of reliable data, and the fulfillment of the (somehow competing) technical needs for a sustainable continuous (24 h per day) monitoring action, on the one hand, and the full-functionality in occasion of rare seismic events, on the other hand. Other major issues regarded the smart design of the hierarchical internal organization of the network. Generalizing the major findings from the specific case-study, the typical geometric and structural configuration of monumental masonry structures, having a dominant wall behaviour, may suggest to organize the sensor sub-groups and the multi-hop communication paths along each longitudinal wall. This conclusion differs from more common cases, like frame buildings, in which a different (floor-based) organization of the sensor groups could be preferable.

Furthermore, the optimization of the network design has highlighted the actual possibility to achieve long-term seismic monitoring with sustainable costs. Indeed, highly-performing expensive sensors may be over-dimensioned in seismic zones, where seismic inputs with sufficient energy content occur with high probability. As a matter of fact, despite a few out-of-service problems occurred during the 3-year monitoring period (2011-present), and despite some unfavorable structural features, structural vibration measurements due to different seismic events have been successfully collected and analyzed.

Based on these data, both direct and inverse problems describing seismic induced structural vibrations have been discussed. In particular, the inverse problem objective was the parametric identification of linear time-invariant state-space models. The effectiveness of input–output and output-only SSI procedures applied to non-stationary (seismic) input data has been evaluated, evidencing the beneficial effect of using base acceleration measures as a deterministic input to which an unmeasured white noise signal is added.

The treatment of data registered during eight different low-energy seismic events has given wide-ranging and valuable information regarding the ability of the SSI methods to extract modal information from noisy acceleration measurements. In particular, the reference-based combined deterministic-SSI technique has been successfully employed in the case of available ground acceleration measurements. The results obtained have been compared with those obtained by output-only procedures (SSI-COV and SSI-DATA) applied to the same data, neglecting knowledge of the input.

About the identification procedure, the research findings clearly evidenced that—in the reference based SSI—the choice of the best-performing and lowest-noisy sensor as reference is of primary importance. Moreover, special care must be taken in the optimal placement of this sensor. From its data, useful information can be extracted, if zero-modal positions are avoided. The procedure robustness has permitted also the identification of the main modal characteristics from the response to seismic events with unknown base acceleration signals. The careful treatment of complementary data acquired by the monitoring system from different excitation sources (release tests, seismic events, etc.) has permitted to update a finite element model of the Basilica in the current damaged conditions. The important role played by the protective systems installed after the partial transept collapse in the complex dynamics of the monument has been highlighted, evidencing some persistent sources of high seismic vulnerability of the church. To date, the wireless sensors' network is continuing to capture the seismic response to very low energy seismic inputs. The assessment of the effectiveness of the protection system and the links between the walls is going on and is under current investigation.

Acknowledgments The research leading to these results has received funding from the Italian Government under Cipe resolution no. 135 (Dec. 21, 2012), project *INnovating City Planning through Information and Communication Technologies*. The authors would like to thank the Italian Ministry of Education, Universities and Research (MIUR) through the PRIN funded program "Dynamics, Stability and Control of Flexible Structures" (grant number 2010MBJK5B).

References

1. Akyldiz IF, Su W, Sankarasubramaniam Y, Cayirci E (2002) Wireless sensor networks: a survey. Comput Netw 38:393–422

2. Spencer BF, Ruiz-Sandoval Manuel E, Kurata N (2004) Smart sensing technology: opportunities and challenges. Struct Control Health Monit 11:349–368
3. Lynch JP, Loh K (2006) A summary review of wireless sensors and sensor networks for structural health monitoring. Shock Vib 38(2):91–128
4. Spencer BF, Chung-Bang Y (eds) (2010) Wireless sensor advances and applications for civil infrastructure monitoring, Newmark Structural Engineering Laboratory Report Series, No. 24. University of Illinois at Urbana-Champaign, Illinois. http://hdl.handle.net/2142/16434, 14 July 2010
5. Zonta D, Wu H, Pozzi M, Zanon P, Ceriotti M, Mottola L, Picco GP, Murphy AL, Guna S, Corrà M (2010) Wireless sensor networks for permanent health monitoring of historic buildings. Smart Struct Syst 6(5–6):595–618
6. Rice JA, Mechitov KA, Sim SH, Spencer BF Jr, Agha GA (2011) Enabling framework for structural health monitoring using smart sensors. Struct Control Health Monit 18:574–587
7. Linderman LE, Mechitov KA, Spencer BF Jr (2013) TinyOS-based real-time wireless data acquisition framework for structural health monitoring and control. Struct Control Health Monit 20(6):1007–1020
8. Capecchi D, Rega G, Vestroni F (1980) A study of the effect of stiffness distribution on nonlinear seismic response of multi-degree-of-freedom structures. Eng Struct 2:244–252
9. Beck JL, Jennings PC (1980) Structural identification using linear models and earthquake records. Earthq Eng Struct Dyn 8(2):145–160
10. Juang JN, Pappa RS (1985) An eigensystem realization algorithm for model parameter identification and model reduction. J Guid Control Dyn 8(5):620–627
11. Ghanem R, Shinozuka M (1995) Structural-system identification. I: theory, II: experimental verification. J Eng Mech ASCE 121(2):255–273
12. Van Overschee P, De Moor B (1996) Subspace identification for linear systems: theory-implementation-applications. Kluwer, Dordrecht
13. Lus H, Betti R, Longman RW (1999) Identification of linear structural systems using earthquake-induced vibration data. Earthq Eng Struct Dyn 28(11):1449–1467
14. Peeters B, De Roeck G (1999) Reference-based stochastic subspace identification for output-only modal analysis. Mech Syst Signal Process 13(6):855–878
15. Peeters B, De Roeck G (2001) Stochastic system identification for operational modal analysis: a review. J Dyn Syst Meas Contr 123(12):659–667
16. Antonacci E, De Stefano A, Gattulli V, Lepidi M, Matta E (2012) Comparative study of vibration-based parametric identification techniques for a three-dimensional frame structure. Struct Control Health Monit 19(5):579–608
17. Reynders E, De Roeck G (2008) Reference-based combined deterministic–stochastic subspace identification for experimental and operational modal analysis. Mech Syst Signal Process 22:617–637
18. Gattulli V, Antonacci E, Vestroni F (2013) Field observations and failure analysis of the basilica S. Maria di Collemaggio after the 2009 L'Aquila earthquake. Eng Fail Anal 34:715–734
19. Brandonisio G, Lucibello G, Mele E, De Luca A (2013) Damage and performance evaluation of masonry churches in the 2009 L'Aquila earthquake. Eng Fail Anal 34:693–714
20. Arcidiacono V, Cimellaro GP, Ochsendorf JA (2015) Analysis of the failure mechanisms of the basilica of Santa Maria di Collemaggio during 2009 L'Aquila earthquake. Eng Struct 99:502–516
21. Amoroso S, Gaudiosi I, Milana G, Tallini M (2013) Preliminary results of seismic response analyses at Santa Maria di Collemaggio Basilica (L'Aquila, Italy). In: Proceedings of 32nd conference Gruppo Nazionale di Geofisica della Terra Solida (GNGTS), Trieste, Italy
22. Ceci AM, Contento A, Fanale L, Galeota D, Gattulli V, Lepidi M, Potenza F (2010) Structural performance of the historic and modern buildings of the University of L'Aquila during the seismic events of April 2009. Eng Struct 32(7):1899–1924
23. Çelebi M (2002) Seismic instrumentation of buildings (with emphasis on federal buildings). Tech. Rep. 0-7460-68170, Geological Survey
24. Russo S (2013) On the monitoring of historic Anime Sante church damaged by earthquake in L'Aquila. Struct Control Health Monit 20(9):1226–1239
25. Russo S (2013) Testing and modelling of dynamic out-of-plane behaviour of the historic masonry facade of Palazzo Ducale in Venice, Italy. Eng Struct 46(1):130–139
26. Pau A, Vestroni F (2013) Vibration assessment and structural monitoring of the Basilica of Maxentius in Rome. Mech Syst Signal Process 41(1–2):454–466
27. Federici F, Graziosi F, Faccio M, Gattulli V, Lepidi M, Potenza F (2012) An integrated approach to the design of wireless sensor networks for structural health monitoring. Int J Distrib Sens Netw. Article ID 594842
28. Lynch JP, Sundararajan A, Law KH, Kiremijdian AS, Carryer E, Sohn H, Farrar CR (2003) Field validation of a wireless structural health monitoring system on the Alamosa Canyon Bridge. Smart Struct Mater 5057:267–278
29. Lynch JP, Wang Y, Law KH, Yi JH, Lee GC, Yun CB (2005) Validation of a large-scale wireless structural monitoring system on the Geumdang Bridge. In: Proceedings of the international conference on safety and structural reliability (ICOSSAR), Rome, Italy
30. Jang S, Jo H, Cho S, Mechitov K, Rice JA, Sim S, Jung H, Yun C, Spencer BF Jr, Agha G (2010) Structural health monitoring of a cable-stayed bridge using smart sensor technology: deployment and evaluation. Smart Struct Syst 6(5–6):439–459
31. Kim S, Pakzad S, Culler D, Demmel J, Fenves G, Glaser S, Turon M (2007) Health monitoring of civil infrastructures using wireless sensor networks. In: Proceedings of the 6th international conference on information processing in sensor networks, Cambridge, Massachusetts
32. Aguilar R, Ramos LF, Lourenco P, Severino R, Gomes R, Gandra P, Alves M, Tovar E (2011) Operational modal monitoring of ancient structures using wireless technology. In: Dynamics of civil structures, conference proceedings of the society for experimental mechanics series 4, pp 247–256
33. Gattulli V, Potenza F, Graziosi F, Federici F, Colarieti A, Faccio M (2014) Design of wireless sensor nodes for structural health monitoring applications. Procedia Eng 87:1298–1301. International the 28th European conference on solid-state transducers, EUROSENSORS 2014, 7–10 Sep 2014, Brescia, Italy
34. Federici F, Alesii R, Colarieti A, Graziosi F, Faccio M (2013) Design and validation of a wireless sensor node for long term structural health monitoring. In: Proceedings of IEEE sensors 2013, Baltimore, USA
35. Gattulli V, Potenza F, Federici F, Graziosi F, Colarieti A, Faccio M (2013) Distributed structural monitoring for a smart city in a seismic area. Key Eng Mater 628:123–135
36. Reynders E, François S, De Roeck G (2009) Operational modal analysis using ambient support excitation: an OMAX approach. In: Proceedings of 3rd international operational modal analysis conference (IOMAC), Portonovo, Italy
37. Kim J, Lynch JP (2012) Subspace system identification of support-excited structures—part I: theory and black box system identification. Earthq Eng Struct Dyn 41:2235–2251
38. Loh CH, Chao SH, Weng JH, Wu TH (2014) Application of subspace identification technique to long-term seismic response

monitoring of structures. Earthq Eng Struct Dyn. doi:10.1002/eqe.2475
39. Siringoringo DM, Fujino Y (2014) Seismic response analyses of an asymmetric base-isolated building during the 2011 Great East Japan (Tohoku) Earthquake. Struct Control Health Monit. doi:10.1002/stc.1661
40. Derkevorkian A, Masri SF, Fijino Y, Siringoringo M (2012) Development and validation of nonlinear computational models of dispersed structures under strong earthquake excitation. Earthq Eng Struct Dyn 43(7):1089–1105
41. Benveniste A, Fuchs JJ (1985) Single sample modal identification of a nonstationary stochastic process. IEEE Trans Autom Control 30(1):66–74
42. Reynders E, Pintelon R, De Roeck G (2008) Uncertainty bounds on modal parameters obtained from stochastic subspace identification. Mech Syst Signal Process 22(4):948–969
43. Foti D, Gattulli V, Potenza F (2014) Output-only identification and model updating by dynamic testing in unfavorable conditions of a seismically damaged building. Comput Aided Civil Infrastruct Eng 29(9):659–675